JACC Vol. 47, No. 9, 2006
May 2, 2006:1882–90

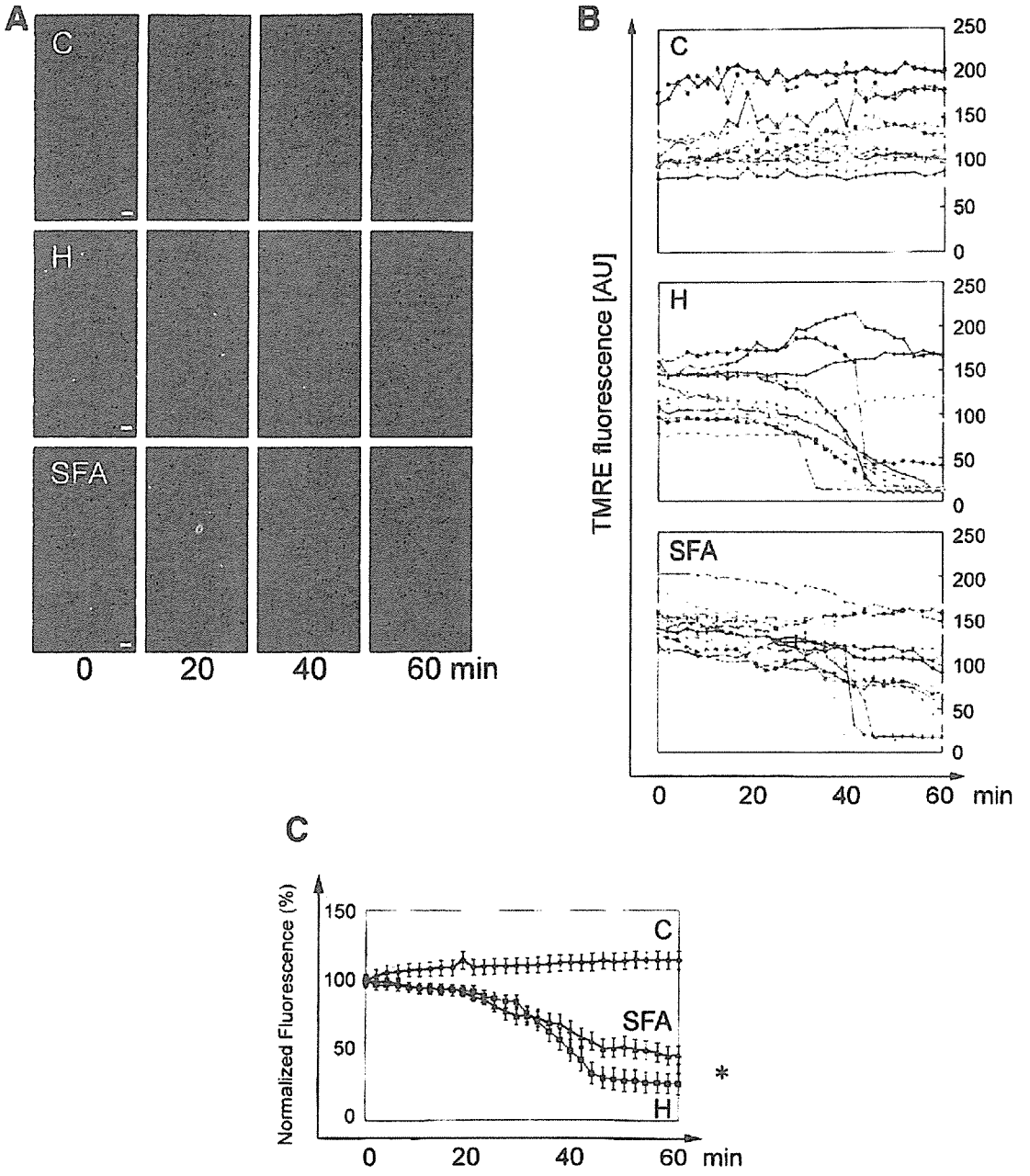

Figure 3. Time-lapse analysis of $\Delta\Psi_m$ loss in neonatal rat cardiac myocytes. **(A)** Representative sequential images of TMRE fluorescence in each group. H = cells exposed to 50 μmol/l H_2O_2 for 1 h; SFA = cells pretreated with 100 μmol/l serofendic acid for 30 min followed by 50 μmol/l H_2O_2 for 1 h. **Scale bars at 0 min frames:** 20 μm. **(B)** Time course of TMRE fluorescence of 25 cells randomly selected in each group. Similar results were obtained in three independent experiments. **(C)** Mean fluorescence intensity from 25 cells randomly and prospectively selected in each group. *$p < 0.05$ versus H at the end of the experimental period. Other abbreviations as in Figure 1. Please see the Appendix for an accompanying video to this figure.

Calcium overload in mitochondrial matrix is one of the critical triggers of cell death and is also an important inducer of MPTP opening. To monitor the $[Ca^{2+}]_m$ level, we performed time-lapse confocal microscopy with the $[Ca^{2+}]_m$ sensitive dye, rhod-2, and observed the change of fluorescence due to 50 μmol/l H_2O_2 stimulation in each group (Fig. 5). We first confirmed that the rhod-2 fluorescence did not change during 60 min of scanning in the control group (Fig. 5A, panels C). In the H_2O_2 group, rhod-2 fluorescence showed pronounced elevation at approximately 20 min after H_2O_2 application, and the elevation persisted thereafter (Fig. 5A, panels H). Serofendic acid also partly attenuated the $[Ca^{2+}]_m$ overload observed in the H_2O_2 group (Fig. 5A, panels SFA). Figure 5B shows the time course of the rhod-2 fluorescence intensity from each individual cell. Serofendic acid blunted the overall increase of rhod-2 fluorescence compared with the H_2O_2 group. Figure 5C shows the average of the rhod-2 fluorescence intensity from 25 randomly selected cells in each group.

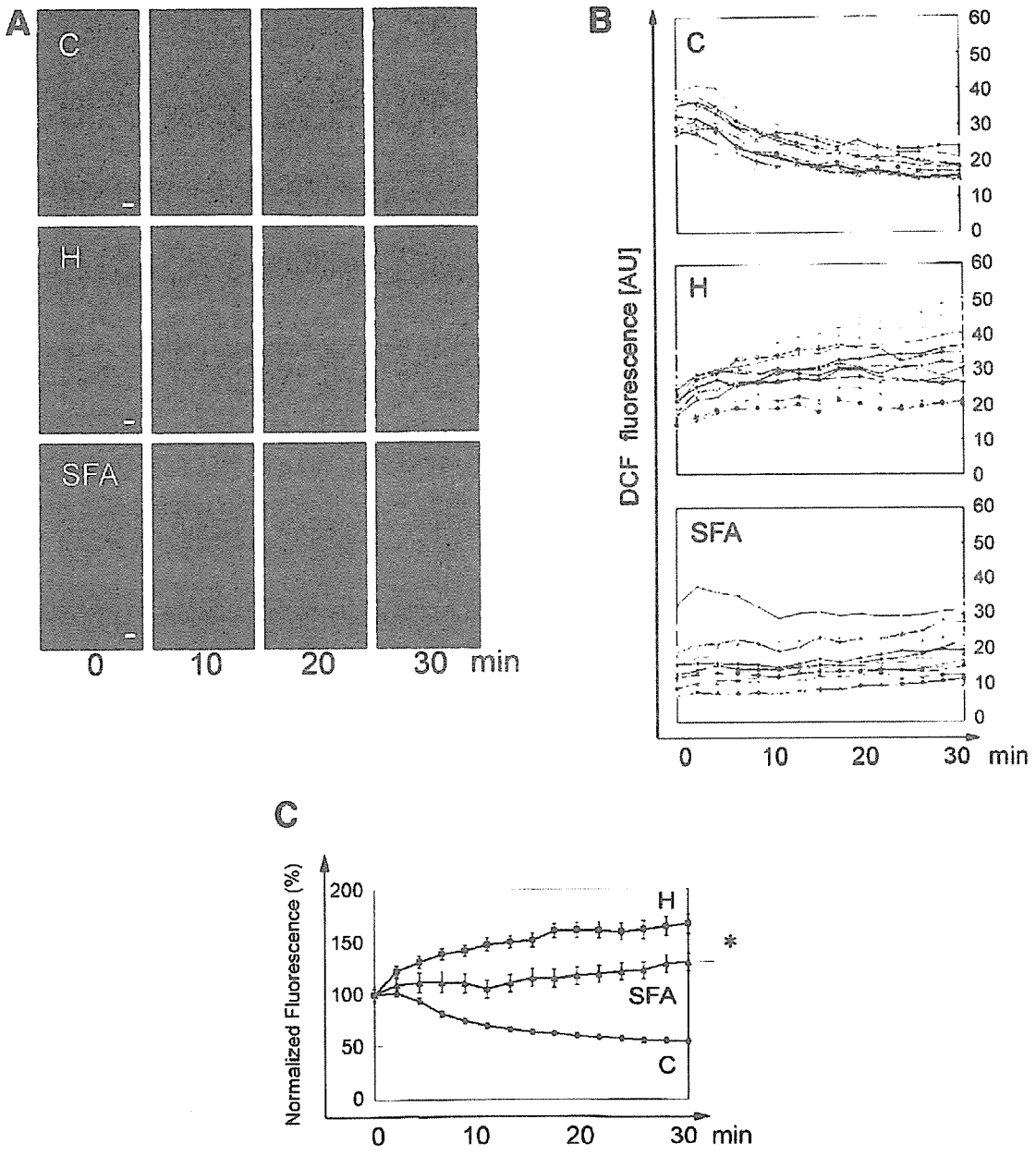

Figure 4. Time-lapse analysis of intracellular reactive oxygen species production in neonatal rat cardiac myocytes. **(A)** Representative sequential images of chloromethyl-2,7-dichlorodihydrofluorescein diacetate (DCF) fluorescence in each group. H = cells exposed to 50 μmol/l H_2O_2 for 30 min; SFA = cells pretreated with 100 μmol/l serofendic acid for 30 min followed by 50 μmol/l H_2O_2 for 30 min. **Scale bars at 0 min frames:** 20 μm. **(B)** Time course of DCF fluorescence of 25 cells randomly selected in each group. Similar results were obtained in three independent experiments. **(C)** Mean fluorescence intensity from 25 cells randomly and prospectively selected in each group. *$p < 0.05$ versus H at the end of the experimental period. Other abbreviations as in Figure 1. Please see the Appendix for an accompanying video to this figure.

DISCUSSION

SFA as a cardioprotective agent. The major findings of this study are as follows. First, in isolated cardiac myocytes, SFA suppressed the cell death induced by H_2O_2 by preserving the $\Delta\Psi_m$ level in a concentration-dependent manner. The preservation of mitochondrial integrity was most likely achieved by the partial inhibition of $[Ca^{2+}]_m$overload and ROS accumulation. Second, serofendic acid and mitoK$_{ATP}$ opener exhibited comparable protective effects, and they did not have an additive beneficial effect on $\Delta\Psi_m$ preservation. MitoK$_{ATP}$ channel blocker 5-HD canceled the protective effect of SFA. These observations suggest that SFA acts either directly on the mitoK$_{ATP}$ channel or, rather, upstream of the mitoK$_{ATP}$ channel.

We previously reported the discovery of the neuroprotective compound SFA, extracted from fetal calf serum (19,20). It is a low molecular weight substance of atisane-type diterpenoids bearing a methylsulfoxide group, a unique chemical structure among known endogenous substances. Our unpublished data (T. Kume, A. Akaike, 2005) show

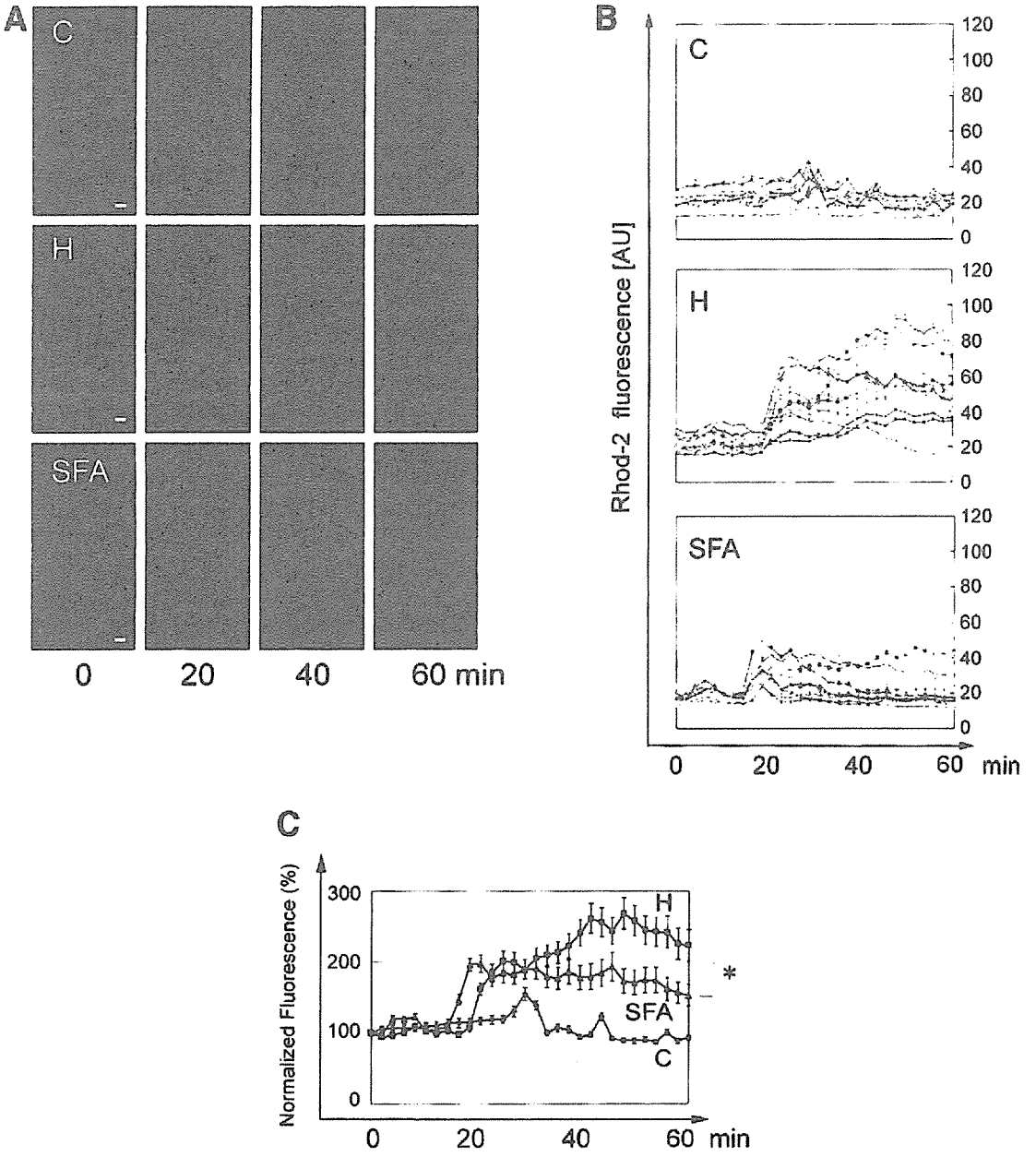

Figure 5. Time-lapse analysis of intracellular mitochondrial matrix calcium in neonatal rat cardiac myocytes. **(A)** Representative sequential images of rhod-2 (Molecular Probes, Eugene, Oregon) fluorescence in each group. H = cells exposed to 50 μmol/l H_2O_2 for 1 h; SFA = cells pretreated with 100 μmol/l serofendic acid for 30 min followed by 50 μmol/l H_2O_2 for 1 h. **Scale bars at 0 min frames:** 20 μm. **(B)** Time course of rhod-2 fluorescence of 25 cells randomly selected in each group. Similar results were obtained in three independent experiments. **(C)** Mean fluorescence intensity from 25 cells randomly and prospectively selected in each group. *$p < 0.05$ versus H at the end of the experimental period. Other abbreviations as in Figure 1. Please see the Appendix for an accompanying video to this figure.

that SFA is contained in fetal calf serum in a considerable amount, but the content in adult bovine is below detectable level. Similarly, we were also unable to detect SFA in adult human serum, although there is a possibility that fetal human serum might contain SFA. The biosynthesis or the metabolism of SFA is unknown at present. Previous studies in vitro indicated that SFA has neuroprotective effects, as evidenced by the prevention of acute glutamate neurotoxicity in cultured cortical neurons (21) and the attenuation of ROS-induced oxidative stress in cultured striatal neurons (22). Suppression of intracellular ROS generation might constitute an important mechanism of the neuroprotective actions of SFA, because the compound exhibits hydroxyl radical-scavenging activity in electron spin resonance analysis (19).

Prevention of MPTP by SFA. In recent studies, ROS generation and $[Ca^{2+}]_m$ overload have been proposed to explain the pathogenesis of ischemia/reperfusion injury of the heart (3,23). Reactive oxygen species and $[Ca^{2+}]_m$ are the most important inducers of MPTP opening. A growing

body of evidence supports the concept that the inhibition of MPTP is an effective and promising strategy to prevent ischemia/reperfusion injury of the heart (3,6,24,25). We clearly showed that SFA prevents MPTP opening, as reported by the preservation of the cell population with fully-polarized (intact) $\Delta\Psi_m$ levels. Notably, SFA only partly suppressed the increases of $[Ca^{2+}]_m$ and ROS, but this partial inhibition might decrease the number of cells that reach the threshold of the catastrophic loss of $\Delta\Psi_m$. This is consistent with the concept that mitochondria are death signal integrators and determine the fate of cells in an all-or-none manner (26).

We have recently shown that oxidant stress produces a stereotyped progression of cellular changes in cardiac myocytes (13). The first phase we call "priming": mitochondria undergo $[Ca^{2+}]_m$-dependent morphological changes, but $\Delta\Psi_m$ remains unchanged. Next follows a sudden dissipation of $\Delta\Psi_m$ mediated by the opening of MPTP ("depolarization" phase); eventually, cells break up into smaller fragments ("fragmentation" phase). Serofendic acid markedly decreased the likelihood that cells would undergo priming: $[Ca^{2+}]_m$ overload was attenuated and, consequently, many mitochondria remained fully polarized. Serofendic acid not only decreased the number of cells undergoing $\Delta\Psi_m$ depolarization but also delayed the onset of $\Delta\Psi_m$ loss, whereas it did not change the duration of depolarization in unprotected cells. This mode of action is equivalent to that of the mitoK$_{ATP}$ channel opener diazoxide (12), raising the possibility that the cytoprotective effects of SFA are directly or indirectly mediated by the mitoK$_{ATP}$ channel. In the present study, we used two different concentrations of H_2O_2:50 μmol/l in confocal time-lapse imaging, and 100 μmol/l for all the other experiments, primarily because the susceptibility of cells to H_2O_2 was dependent on the plating surface. We have confirmed that cells underwent similar three-step progression of cell death in an all-or-none manner, even when they were exposed to lower concentrations of H_2O_2 (13).

SFA and mitoK$_{ATP}$ channel. It is clear that a cardioprotective effect can be recruited by mitoK$_{ATP}$ channel openers, and mitoK$_{ATP}$ channel blockers (5-HD or glibenclamide) prevent both preconditioning and pharmacological cardioprotection (27–29). Furthermore, mitoK$_{ATP}$ channel opening prevents mitochondrial injury, presumably by inhibiting the opening of MPTP (12,13). MitoK$_{ATP}$ channel activation induces partial and modest $\Delta\Psi_m$ depolarization, thereby reducing the driving force for calcium uptake by mitochondria and preventing $[Ca^{2+}]_m$ elevation (14). This is further supported by the observation that partial $\Delta\Psi_m$ depolarization elicited by the overexpression of uncoupling protein-2 also protected cardiac myocytes (30). In this study, the protective effect of SFA was comparable to that of diazoxide, and the co-application with SFA and diazoxide did not show an additive effect. Furthermore, the mitoK$_{ATP}$ channel blocker, 5-HD, abolished the protective effect of SFA. These results strongly suggest that the protective effect of SFA might be mediated by the activation of mitoK$_{ATP}$ channels. Nevertheless, we could not rule out the possibility that SFA might act on the surface membrane potential of cardiomyocytes and reduce cytosolic calcium overload.

Clinical implications. Many pharmacological agents and strategies have been administered for cardiac protection during acute myocardial infarction (31); however, none have been translated into clinical practice (32). Therapeutic interventions designed to prevent MPTP opening during ischemia/reperfusion hold major promise as a novel strategy for reducing cardiac injury from ischemia/reperfusion (6). Our findings suggest SFA as a novel candidate for cardioprotective therapy against ischemia/reperfusion injury. Serofendic acid is expected to be free from unpredictable side effects, because it is an endogenous substance. Despite the positive prospect of SFA as a novel cardioprotective agent, further investigations in animal models are needed to assess the infarct size-limiting effect.

Reprint requests and correspondence: Dr. Masaharu Akao, Department of Cardiovascular Medicine, Kyoto University Graduate School of Medicine, 54 Kawahara-cho, Shogoin, Sakyo-ku, Kyoto 606-8507, Japan. E-mail: akao@kuhp.kyoto-u.ac.jp.

REFERENCES

1. Green DR, Kroemer G. The pathophysiology of mitochondrial cell death. Science 2004;305:626–9.
2. Kroemer G, Dallaporta B, Resche-Rigon M. The mitochondrial death/life regulator in apoptosis and necrosis. Annu Rev Physiol 1998;60:619–42.
3. Weiss JN, Korge P, Honda HM, Ping P. Role of the mitochondrial permeability transition in myocardial disease. Circ Res 2003;93:292–301.
4. Crompton M. The mitochondrial permeability transition pore and its role in cell death. Biochem J 1999;341:233–49.
5. Crow MT, Mani K, Nam YJ, Kitsis RN. The mitochondrial death pathway and cardiac myocyte apoptosis. Circ Res 2004;95:957–70.
6. Halestrap AP, Clarke SJ, Javadov SA. Mitochondrial permeability transition pore opening during myocardial reperfusion—a target for cardioprotection. Cardiovasc Res 2004;61:372–85.
7. Brookes PS, Yoon Y, Robotham JL, Anders MW, Sheu SS. Calcium, ATP, and ROS: a mitochondrial love-hate triangle. Am J Physiol Cell Physiol 2004;287:C817–33.
8. Akao M, Ohler A, O'Rourke B, Marban E. Mitochondrial ATP-sensitive potassium channels inhibit apoptosis induced by oxidative stress in cardiac cells. Circ Res 2001;88:1267–75.
9. Akao M, Teshima Y, Marban E. Antiapoptotic effect of nicorandil mediated by mitochondrial ATP-sensitive potassium channels in cultured cardiac myocytes. J Am Coll Cardiol 2002;40:803–10.
10. Teshima Y, Akao M, Li RA, et al. Mitochondrial ATP-sensitive potassium channel activation protects cerebellar granule neurons from apoptosis induced by oxidative stress. Stroke 2003;34:1796–802.
11. Teshima Y, Akao M, Baumgartner WA, Marban E. Nicorandil prevents oxidative stress-induced apoptosis in neurons by activating mitochondrial ATP-sensitive potassium channels. Brain Res 2003;990:45–50.
12. Akao M, O'Rourke B, Kusuoka H, Teshima Y, Jones SP, Marban E. Differential actions of cardioprotective agents on the mitochondrial death pathway. Circ Res 2003;92:195–202.
13. Akao M, O'Rourke B, Teshima Y, Seharaseyon J, Marban E. Mechanistically distinct steps in the mitochondrial death pathway triggered by oxidative stress in cardiac myocytes. Circ Res 2003;92:186–94.

14. Murata M, Akao M, O'Rourke B, Marban E. Mitochondrial ATP-sensitive potassium channels attenuate matrix Ca^{2+} overload during simulated ischemia and reperfusion: possible mechanism of cardioprotection. Circ Res 2001;89:891–8.
15. Garlid KD, Paucek P, Yarov-Yarovoy V, et al. Cardioprotective effect of diazoxide and its interaction with mitochondrial ATP-sensitive K^+ channels. Possible mechanism of cardioprotection. Circ Res 1997;81:1072–82.
16. Liu Y, Sato T, O'Rourke B, Marban E. Mitochondrial ATP-dependent potassium channels: novel effectors of cardioprotection? Circulation 1998;97:2463–9.
17. Fryer RM, Eells JT, Hsu AK, Henry MM, Gross GJ. Ischemic preconditioning in rats: role of mitochondrial K_{ATP} channel in preservation of mitochondrial function. Am J Physiol Heart Circ Physiol 2000;278:H305–12.
18. Miura T, Liu Y, Kita H, Ogawa T, Shimamoto K. Roles of mitochondrial ATP-sensitive K channels and PKC in anti-infarct tolerance afforded by adenosine A1 receptor activation. J Am Coll Cardiol 2000;35:238–45.
19. Kume T, Asai N, Nishikawa H, et al. Isolation of a diterpenoid substance with potent neuroprotective activity from fetal calf serum. Proc Natl Acad Sci U S A 2002;99:3288–93.
20. Akaike A, Katsuki H, Kume T. Pharmacological and physiological properties of serofendic acid, a novel neuroprotective substance isolated from fetal calf serum. Life Sci 2003;74:263–9.
21. Taguchi R, Nishikawa H, Kume T, et al. Serofendic acid prevents acute glutamate neurotoxicity in cultured cortical neurons. Eur J Pharmacol 2003;477:195–203.
22. Osakada F, Kawato Y, Kume T, Katsuki H, Sugimoto H, Akaike A. Serofendic acid, a sulfur-containing diterpenoid derived from fetal calf serum, attenuates reactive oxygen species-induced oxidative stress in cultured striatal neurons. J Pharmacol Exp Ther 2004;311:51–9.
23. Griendling KK, Alexander RW. Oxidative stress and cardiovascular disease. Circulation 1997;96:3264–5.
24. Murphy E. Primary and secondary signaling pathways in early preconditioning that converge on the mitochondria to produce cardioprotection. Circ Res 2004;94:7–16.
25. Hausenloy DJ, Duchen MR, Yellon DM. Inhibiting mitochondrial permeability transition pore opening at reperfusion protects against ischaemia-reperfusion injury. Cardiovasc Res 2003;60:617–25.
26. Brenner C, Kroemer G. Apoptosis. Mitochondria—the death signal integrators.Science 2000;289:1150–1.
27. Gross GJ. ATP-sensitive potassium channels and myocardial preconditioning. Basic Res Cardiol 1995;90:85–8.
28. O'Rourke B. Myocardial K_{ATP} channels in preconditioning. Circ Res 2000;87:845–55.
29. O'Rourke B. Evidence for mitochondrial K^+ channels and their role in cardioprotection. Circ Res 2004;94:420–32.
30. Teshima Y, Akao M, Jones SP, Marban E. Uncoupling protein-2 overexpression inhibits mitochondrial death pathway in cardiomyocytes. Circ Res 2003;93:192–200.
31. Kloner RA, Rezkalla SH. Cardiac protection during acute myocardial infarction: where do we stand in 2004? J Am Coll Cardiol 2004;44:276–86.
32. Bolli R, Becker L, Gross G, Mentzer R Jr., Balshaw D, Lathrop DA. Myocardial protection at a crossroads: the need for translation into clinical therapy. Circ Res 2004;95:125–34.

APPENDIX

For accompanying videos to Figures 3, 4, and 5, please see the online version of this article.

Uterine sensitization-associated gene–1 (USAG-1), a novel BMP antagonist expressed in the kidney, accelerates tubular injury

Motoko Yanagita,[1] Tomohiko Okuda,[1] Shuichiro Endo,[2] Mari Tanaka,[2] Katsu Takahashi,[3] Fumihiro Sugiyama,[4] Satoshi Kunita,[4] Satoru Takahashi,[4] Atsushi Fukatsu,[5] Masashi Yanagisawa,[6,7] Toru Kita,[2] and Takeshi Sakurai[6,8]

[1]COE Formation for Genomic Analysis of Disease Model Animals with Multiple Genetic Alterations, [2]Department of Cardiovascular Medicine, and [3]Department of Oral and Maxillofacial Surgery, Graduate School of Medicine, Kyoto University, Kyoto, Japan. [4]Laboratory Animal Resource Center, Institute of Basic Medical Sciences, University of Tsukuba, Ibaraki, Japan. [5]Department of Artificial Kidneys, Graduate School of Medicine, Kyoto University, Kyoto, Japan. [6]Yanagisawa Orphan Receptor Project, Exploratory Research for Advanced Technology (ERATO), Japan Science and Technology Agency, Tokyo, Japan. [7]Howard Hughes Medical Institute and Department of Molecular Genetics, University of Texas Southwestern Medical Center, Dallas, Texas, USA. [8]Department of Pharmacology, Institute of Basic Medical Sciences, University of Tsukuba, Ibaraki, Japan.

Dialysis dependency is one of the leading causes of morbidity and mortality in the world, and once end-stage renal disease develops, it cannot be reversed by currently available therapy. Although administration of large doses of bone morphogenetic protein–7 (BMP-7) has been shown to repair established renal injury and improve renal function, the pathophysiological role of endogenous BMP-7 and regulatory mechanism of its activities remain elusive. Here we show that the product of *uterine sensitization-associated gene–1* (*USAG1*), a novel BMP antagonist abundantly expressed in the kidney, is the central negative regulator of BMP function in the kidney and that mice lacking USAG-1 (*USAG1*$^{-/-}$ mice) are resistant to renal injury. *USAG1*$^{-/-}$ mice exhibited prolonged survival and preserved renal function in acute and chronic renal injury models. Renal BMP signaling, assessed by phosphorylation of Smad proteins, was significantly enhanced in *USAG1*$^{-/-}$ mice with renal injury, indicating that the preservation of renal function is attributable to enhancement of endogenous BMP signaling. Furthermore, the administration of neutralizing antibody against BMP-7 abolished renoprotection in *USAG1*$^{-/-}$ mice, indicating that USAG-1 plays a critical role in the modulation of renoprotective action of BMP and that inhibition of USAG-1 is a promising means of development of novel treatment for renal diseases.

Introduction

Despite a significant increase in understanding of the pathophysiology of renal diseases, the incidence of end-stage renal disease (ESRD) is still increasing. Tubular damage and interstitial fibrosis are the final common pathway leading to ESRD (1, 2), irrespective of the nature of the initial renal injury, and the degree of tubular damage parallels the impairment of renal function (2). Once tubular damage is established, it cannot be reversed or repaired by currently available treatment, and renal function deteriorates to renal failure, which is often life threatening (3). If we can come up with an agent that can reverse established tubular damage, it would significantly reduce the need for dialysis. Bone morphogenetic protein-7 (BMP-7) is a promising candidate for such an agent, because it is reported to protect the kidney from renal injury (4–8). BMP-7 is known to play essential roles in kidney development, because BMP-7–null mice die shortly after birth due to severe renal hypoplasia (9, 10). BMP-7 is also abundant in the adult kidney, especially in distal tubule epithelial cells (11, 12). Recently, several reports indicated that the expression of BMP-7 is decreased in renal disease models (5, 6, 13–16) and that administration of recombinant BMP-7 at pharmacological doses repairs chronic renal injury (4–8). However, the pathophysiological role and regulatory mechanism of endogenous BMP-7 remain elusive.

The local activity of endogenous BMP is controlled not only by regulation of its expression, but also by certain classes of molecules termed BMP antagonists (17). BMP antagonists function through direct association with BMP, thus inhibiting the binding of BMP to its receptors. *Uterine sensitization-associated gene–1* (*USAG1*) encodes a secreted protein and was initially found as a gene of unknown function whose expression was upregulated in sensitized endometrium of the rat uterus (18). Recently, Avsian-Kretchmer et al. suggested USAG-1 as a candidate for a novel BMP antagonist using bioinformatic analysis (19). Furthermore, Laurikkala et al. demonstrated USAG-1 to be a BMP antagonist expressed in teeth (20).

We independently identified USAG-1 to be a novel BMP antagonist, abundantly expressed in the kidney (21). The expression of USAG-1 is abundant in renal tubules and teeth in late embryogenesis and in adult tissues it is by far most abundant in the kidney, especially in the distal tubule with a pattern similar to that of BMP-7. From these findings, we hypothesized that USAG-1 might regulate the renoprotective action of BMP-7 in the adult kidney.

To evaluate this hypothesis, we generated *USAG1*-knockout (*USAG1*$^{-/-}$) mice and induced acute and chronic renal disease models in which renal tubules, but not glomeruli, were mainly damaged.

Nonstandard abbreviations used: BMP-7, bone morphogenetic protein-7; EMT, epithelial-mesenchymal transition; MCP-1, monocyte chemotactic protein-1; PTEC, proximal tubule epithelial cell; USAG1, uterine sensitization-associated gene-1; UUO, unilateral ureteral obstruction.

Conflict of interest: The authors have declared that no conflict of interest exists.

Citation for this article: *J. Clin. Invest.* **116**:70–79 (2006). doi:10.1172/JCI25445.

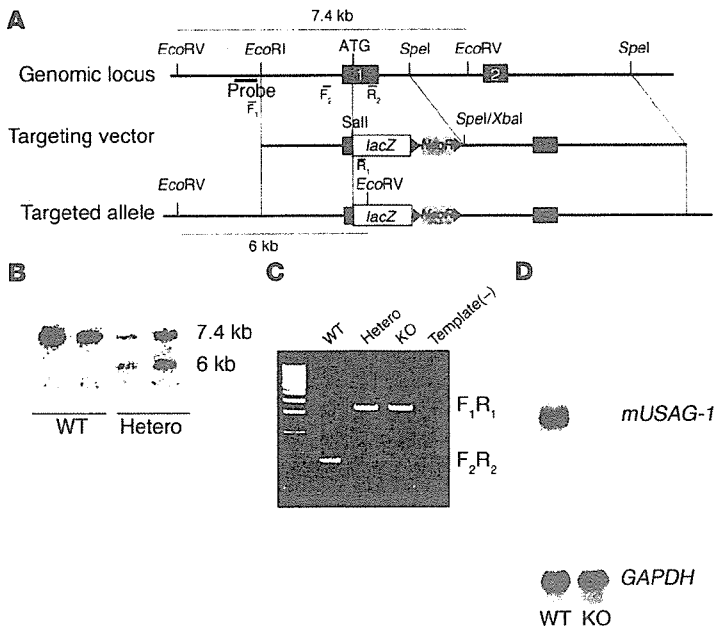

Figure 1
Generation of *USAG1*$^{-/-}$ mutation by gene targeting. (**A**) *USAG1*–null allele was generated by homologous recombination in ES cells. Exon 1 (black box) and part of the intron were replaced with a *lacZ* gene (white box) and the *Neo*R cassette (gray box). (**B**) Analysis of *USAG1*$^{+/+}$ (WT) and correctly targeted heterozygous (Hetero) ES cell clones by Southern blot analysis using 5′ genomic probe (thick black line in **A**). (**C**) PCR genotyping of F_2 littermates. Template(–) is the negative control. (**D**) Northern blot analysis of *USAG1* mRNA in the kidney of *USAG1*$^{+/+}$ and *USAG1*$^{-/-}$ (KO) mice.

Results

Generation and analysis of USAG1$^{-/-}$ *mice.* *USAG1*$^{-/-}$ mice were generated by deleting the first exon including the transcription initiation codon, the signal peptide, and the following 46 amino acids (Figure 1). *USAG1*$^{-/-}$ mice were born at the ratio expected according to Mendel's law of heredity and were viable, fertile, and appeared healthy except that they exhibited supernumerary teeth, both in the incisors and molars, and fused teeth in the molar region (Supplemental Figure 1; supplemental material available online with this article; doi:10.1172/JCI25445DS1). Although there was variation in the sites of extra teeth and fused teeth, this tooth phenotype was fully penetrant. Food consumption was not disturbed by this tooth phenotype in *USAG1*$^{-/-}$ mice (data not shown).

Attenuated acute tubular injury in USAG1$^{-/-}$ *mice.* To induce acute tubular injury, we utilized a cisplatin nephrotoxicity model (22–24). Administration of a nephrotoxic agent, cisplatin, to wild-type littermates caused acute tubular injury that resulted in severe renal failure. Within the first 3 days, 54% of wild-type mice died, while 92% of *USAG1*$^{-/-}$ mice survived the period (Figure 2A). The renal function of *USAG1*$^{-/-}$ mice on day 3 was significantly preserved compared with that in wild-type littermates (Figure 2B). Histological examination of the kidneys of wild-type mice on day 3 showed severe proximal tubular damage, while this change was markedly reduced in *USAG1*$^{-/-}$ mice (Figure 2, C and D). Expression of E-cadherin, a marker for tubular epithelial integrity (25), was markedly reduced in the kidneys of wild-type mice, while its expression was preserved in *USAG1*$^{-/-}$ mice (Figure 2E). Tubular apoptosis, a characteristic feature of tubular injury in cisplatin nephrotoxicity (23), was also significantly reduced in *USAG1*$^{-/-}$ mice (Figure 2F). As reported previously (24), cisplatin administration resulted in upregulation of TNF-α, IL-1β, monocyte chemotactic protein-1 (MCP-1), TGF-β1, and type IV collagen expression in the kidney of wild-type mice. However, the induction of these genes was completely abolished in *USAG1*$^{-/-}$ mice (Figure 2G). Infiltration of macrophages and monocytes in the kidney was also significantly reduced in *USAG1*$^{-/-}$ mice (Figure 2H), in accordance with the reduction of MCP-1 expression (Figure 2G). Expression of BMP-7 was comparable between wild-type mice and *USAG1*$^{-/-}$ mice before and after injection of cisplatin (Figure 2G).

Renal fibrosis is reduced in USAG1$^{-/-}$ *mice.* As a model of chronic renal injury, we performed unilateral ureteral obstruction (UUO) (26, 27) in both *USAG1*$^{-/-}$ mice and wild-type mice, and the kidneys were harvested 14 days after the operation. In wild-type mice, the obstructed kidney showed dilatation/degeneration of renal tubules and interstitial fibrosis, whereas the normal architecture was preserved in *USAG1*$^{-/-}$ mice, except for mild dilatation of tubules (Figure 3, A and B). Expression of E-cadherin was markedly reduced in the kidneys of wild-type mice, while its expression was preserved in *USAG1*$^{-/-}$ mice (Figure 3C). Furthermore, expression of α-SMA, a marker of tubulointerstitial myofibroblasts (28), was upregulated in the interstitium of the obstructed kidney of wild-type mice, while high expression of α-SMA was restricted to vascular smooth muscle cells in *USAG1*$^{-/-}$ mice (Figure 3D). Since expansion and fibrosis of the renal interstitium is another characteristic feature of UUO (6), we examined the deposition of type IV collagen, which is a normal component of the tubular basement membrane. The basement membranes of neighboring tubules are adjacent to each other in the normal kidney. In the obstructed kidney of wild-type mice, expansion of the interstitial component increased the distance between adjacent basement membranes, and type IV collagen produced by interstitial myofibroblasts was aberrantly expressed in the interstitium. However, in the obstructed kidney of *USAG1*$^{-/-}$ mice, the distance between the basement membranes was significantly smaller than that in wild-type mice (Figure 3E). Expression of TNF-α, IL-1β, MCP-1, TGF-β1, and type IV collagen was markedly upregulated on day 14 in the obstructed kidney of wild-type mice. In contrast, the induction of these genes was significantly attenuated, by 33%, 46%, 37%, 75%, and 23%, respectively, in *USAG1*$^{-/-}$ mice (Figure 3F). Expression of BMP-7 in the obstructed kidney was comparable in wild-type mice and *USAG1*$^{-/-}$ mice.

BMP signaling is enhanced in USAG1$^{-/-}$ *mice.* To evaluate whether the reduction in renal injury in *USAG1*$^{-/-}$ mice is attributable to enhanced BMP signaling, phosphorylation of Smad1/5/8 in the kidney was examined in both models (Figure 4). After the induction of kidney disease models, phosphorylation of Smad1/5/8 was hardly detected in wild-type mice, while in *USAG1*$^{-/-}$mice, the phosphorylation was preserved in the nuclei of tubular epithelial cells (Figure 4A). To examine the specificity of the antibody against phospho-Smad1/5/8, we performed double immunostaining using anti-phospho-Smad1/5/8 antibody and anti-phospho-Smad2/3, and found that most of the nuclei positive for phospho-Smad1/5/8 were negative for phospho-Smad2/3 (Figure 4B), indicating the

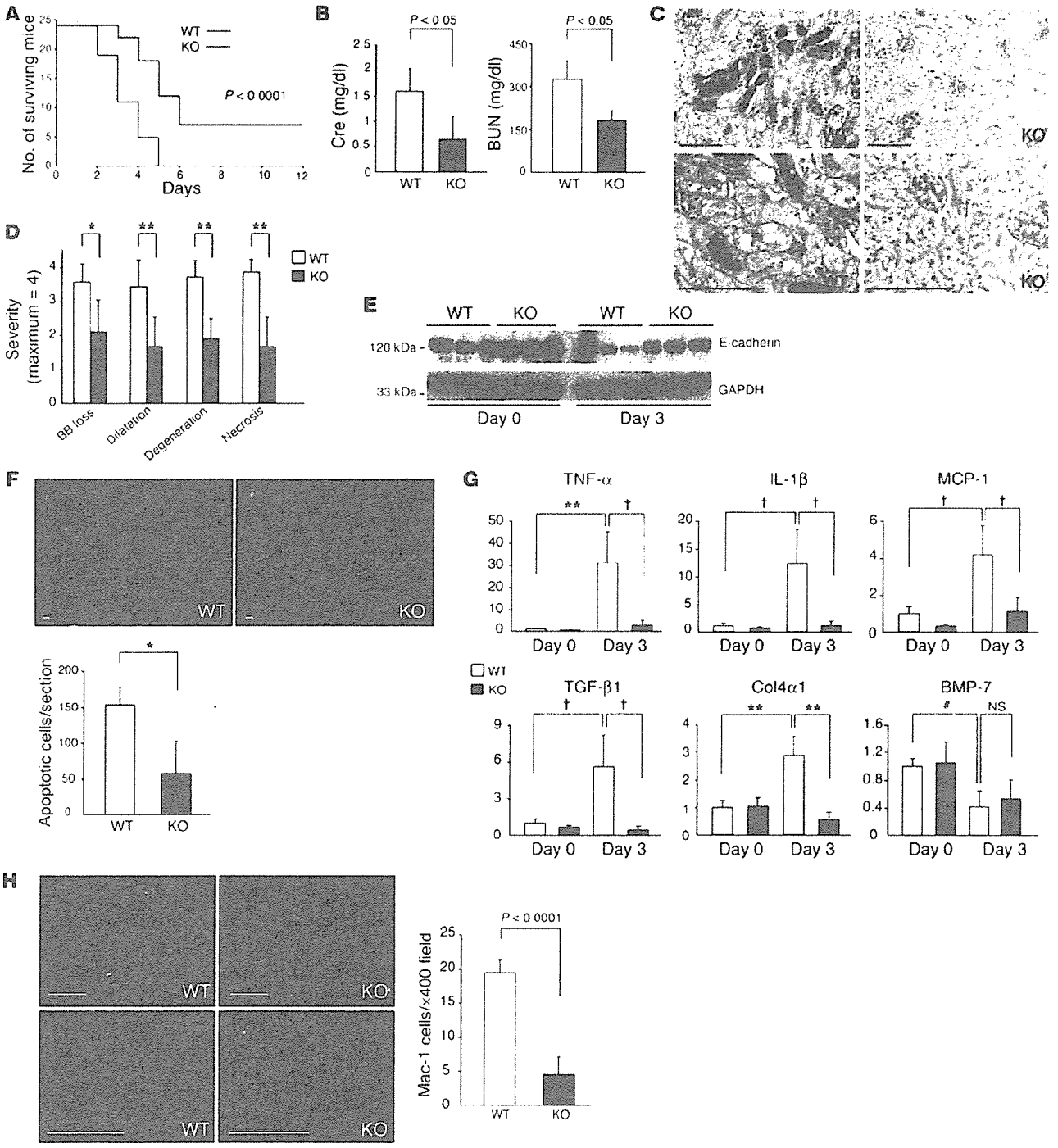

Figure 2

USAG1$^{-/-}$ mice showed less renal injury in cisplatin nephrotoxicity. (**A**) Survival curves of wild-type mice (black line) and *USAG1*$^{-/-}$ mice (red line) after cisplatin administration ($n = 24$). (**B**) Serum creatinine (Cre) and blood urea nitrogen (BUN) levels at 3 days after injection of cisplatin ($n = 6$). (**C**) Representative renal histological findings in wild-type mice and *USAG1*$^{-/-}$ mice on day 3. Scale bars: 100 μm. (**D**) Semiquantitative evaluation of morphologic kidney damage, expressed as relative severity on a scale from 0 to 4 ($n = 6$). Morphological findings were scored according to proximal tubule brush border loss (BB loss), tubule dilatation (Dilatation), tubule degeneration (Degeneration), and tubule necrosis (Necrosis). $^{*}P < 0.01$; $^{**}P < 0.001$. (**E**) E-cadherin expression in cisplatin nephrotoxicity. Kidney lysates were subjected to immunoblotting with anti–E-cadherin antibody. Representative data from 4 independent experiments are shown. (**F**) TUNEL staining of kidneys on day 3 of cisplatin nephrotoxicity. The number of TUNEL-positive cells per section was counted in transverse sections ($n = 6$). Scale bars: 10 μm. (**G**) Gene expression in cisplatin nephrotoxicity. Gene expression was determined by real-time RT-PCR. In each experiment, expression levels were normalized to the expression of GAPDH and expressed relative to mice on day 0. $n = 4$–6 for each experiment. $^{\dagger}P < 0.005$; $^{\#}P < 0.02$. Col4α1, collagen type IV α 1. (**H**) Infiltration of Mac-1–positive cells after cisplatin injection. The number of Mac-1–positive cells per field was counted in 10 consecutive fields ($n = 6$). Scale bars: 100 μm.

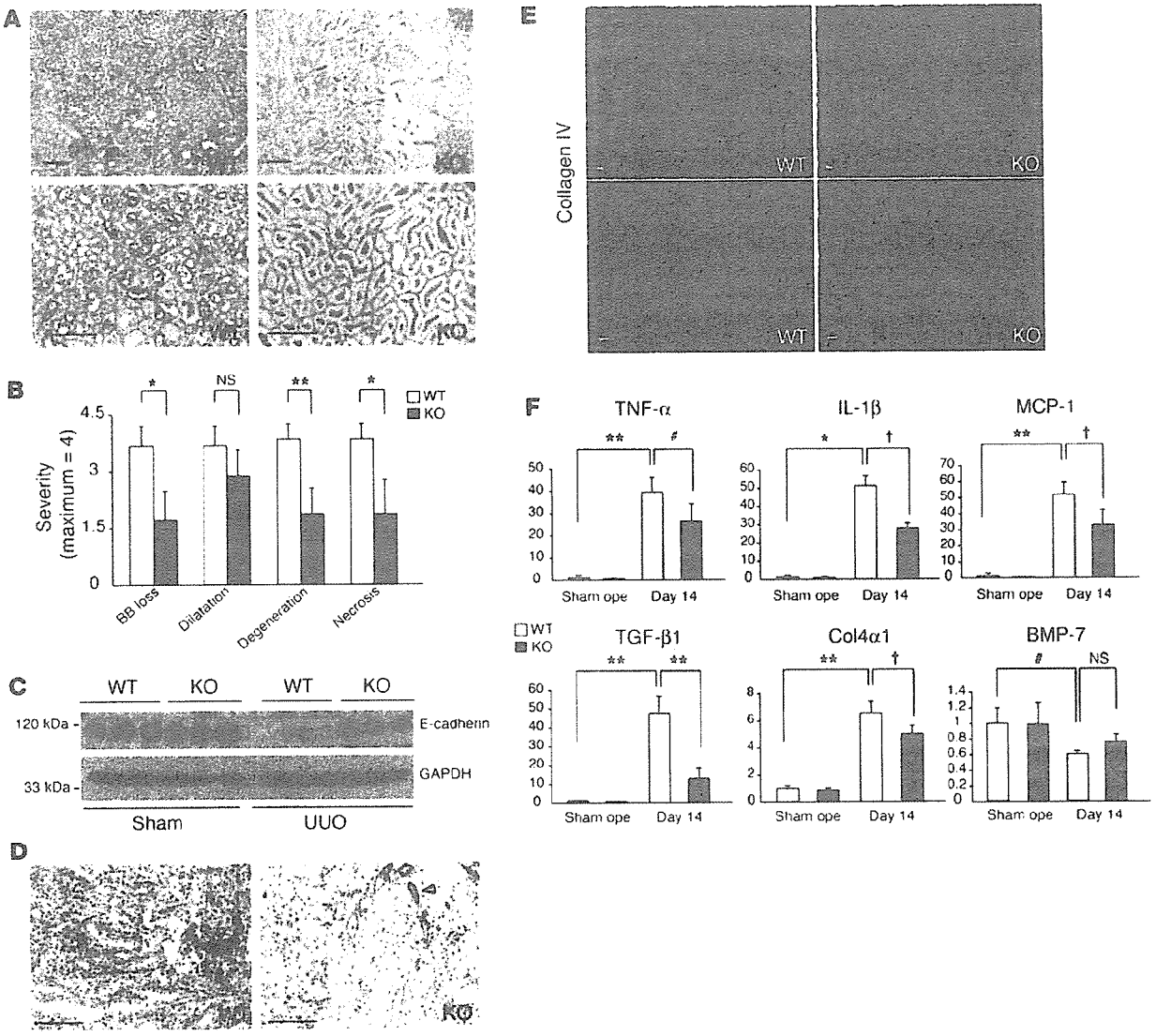

Figure 3

USAG1$^{-/-}$ mice showed reduced EMT and tubulointerstitial fibrosis in UUO. (**A**) Representative histology of the obstructed kidney in wild-type mice and *USAG1*$^{-/-}$ mice 14 days after the operation. Scale bars: 100 μm. (**B**) Semiquantitative evaluation of morphologic kidney damage in wild-type mice and *USAG1*$^{-/-}$ mice, expressed as relative severity on a scale from 0 to 4 (n = 6). (**C**) E-cadherin expression in UUO. Kidney lysates were subjected to immunoblotting with anti–E-cadherin antibody. Representative data from 4 independent experiments are shown. (**D**) Immunostaining of α-SMA in UUO. Arrowheads indicate vascular smooth muscle cells. (**E**) Immunostaining of type IV collagen in UUO. Scale bars: 10 μm. (**F**) Gene expression in UUO. Gene expression was determined by real-time RT-PCR. In each experiment, the expression levels were normalized to the expression of GAPDH and expressed relative to expression in mice on day 0. n = 4–6 for each experiment. $^{\#}P < 0.01$; $^{\dagger}P < 0.005$; $^{*}P < 0.001$; $^{**}P < 0.0001$. Sham ope, mice 14 days after sham operation; day 14, mice 14 days after UUO.

specificity of the antibody against phospho-Smad1/5/8. We also examined the phosphorylation of Smad1/5/8 in immunoblotting of kidney lysates and demonstrated that the phosphorylation was preserved in the kidneys of *USAG1*$^{-/-}$ mice, while it was downregulated in WT mice (Figure 4C). No difference was observed in the phosphorylation of Smad1/5/8 prior to disease induction between *USAG1*$^{-/-}$ mice and WT mice (Figure 4, A and C).

Blocking BMP-7 activity abolishes renoprotection in USAG1$^{-/-}$*mice.* To analyze the mechanism of renoprotection in *USAG1*$^{-/-}$mice, we administered a neutralizing antibody against BMP-7 to *USAG1*$^{-/-}$ mice in both kidney disease models. First we evaluated the specificity of the neutralizing activity of the antibody using an assay measuring alkaline phosphatase activity and phosphorylation of Smad1/5/8 in C2C12 cells induced by BMPs. Addition of the antibody inhibited the alkaline phosphatase activity and phosphorylation of Smad1/5/8 induced by BMP-7, but not by BMP-4 (Figure 5A) or BMP-2 (data not shown), indicating the specificity of the antibody. As a negative control, we used isotype-matched IgG2B. Next we administered a neutralizing antibody against BMP-7 to *USAG1*$^{-/-}$ mice with cisplatin nephrotoxicity. Of 7 mice treated with neutralizing antibody, 2 mice died on day 2 and 1 mouse died on day 3, while none of the mice treated with isotype-matched IgG2B

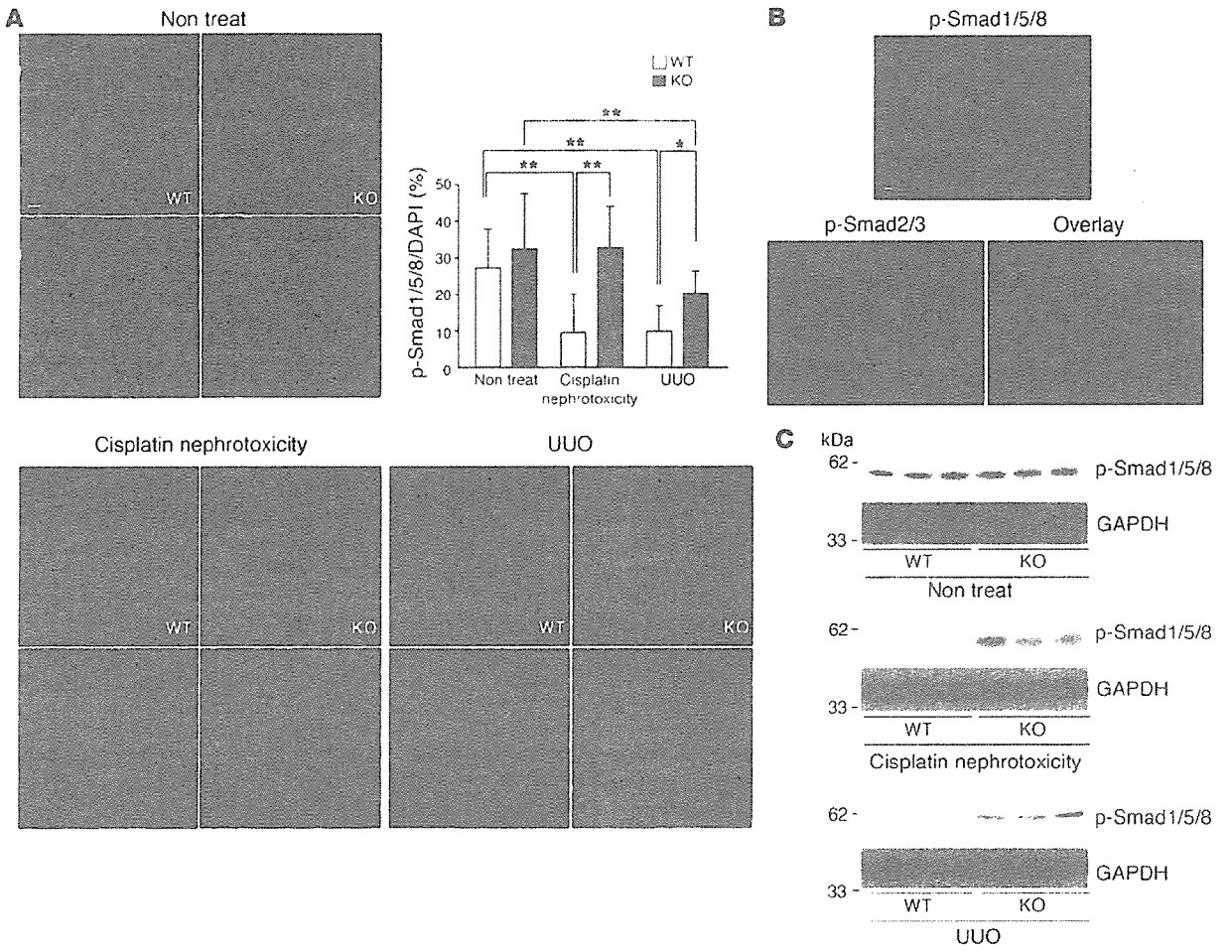

Figure 4
Enhanced BMP signaling in kidneys of *USAG1*$^{-/-}$ mice. (**A**) Phosphorylation of Smad1/5/8 in kidneys of *USAG1*$^{-/-}$ mice and WT mice. The number of pSmad1/5/8-positive nuclei (upper panels) was counted in 10 consecutive fields in each specimen and normalized by the number of DAPI-positive nuclei (lower panels). $n = 6$. Scale bar: 10 μm. $^{*}P < 0.001$; $^{**}P < 0.0001$. Non treat, mice without disease models. (**B**) Double immunostaining of phospho-Smad1/5/8 and phospho-Smad2/3. Almost all the nuclei positive for pSmad1/5/8 were negative for pSmad2/3. Scale bar: 10 μm. (**C**) Immunoblotting of phospho-Smad1/5/8 in kidney lysates prior to disease induction and in both kidney disease models. Representative data from 5 independent experiments are shown.

died within the first 3 days. Administration of neutralizing antibody also resulted in a deterioration of renal function measured by elevation of serum creatinine to a level similar to that in WT mice, while administration of IgG2B did not (Figure 5B). Furthermore, histological examination of the kidneys of *USAG1*$^{-/-}$ mice treated with neutralizing antibody demonstrated severely damaged proximal tubular epithelial cells, while these changes were absent in mice treated with IgG2B (Figure 5B). We also administered the neutralizing antibody to *USAG1*$^{-/-}$ mice with UUO and found that type IV collagen expression in the obstructed kidney was increased in *USAG1*$^{-/-}$ mice treated with neutralizing antibody, but not in those administered IgG2B (Figure 5C). Histological examination of the obstructed kidneys of *USAG1*$^{-/-}$ mice treated with neutralizing antibody demonstrated severe interstitial fibrosis, while this change was almost absent in mice treated with IgG2B (Figure 5C).

USAG1 is the most abundant BMP antagonist in adult kidney. Finally we analyzed the expression of USAG-1 and other BMP antagonists in adult kidneys using modified real-time PCR and in situ hybridization (Figure 6). To compare the expression levels of different genes in real-time PCR, we set the standard curve with the plasmid encoding each BMP antagonist at various concentrations and analyzed the copy number of each gene contained in kidney cDNA. Among known BMP antagonists, USAG-1 was by far the most abundant in the kidneys, and twisted gastrulation was the second most abundant BMP antagonist. We also analyzed the localization of BMP antagonists in the kidneys using in situ hybridization and found that the expression of USAG-1 was confined to distal tubules, as previously described (21), with a pattern similar to that of BMP-7 (12). Expression of twisted gastrulation was also detected in some distal tubules; however, the intensity of the signal was much lower than that of USAG-1, in accordance with the results of real-time PCR. Differential screening-selected gene aberrative in neuroblastoma (DAN) and protein related to DAN and Cerberus (PDRC) were faintly observed in the inner medulla, and other BMP antagonists were not detected with this method.

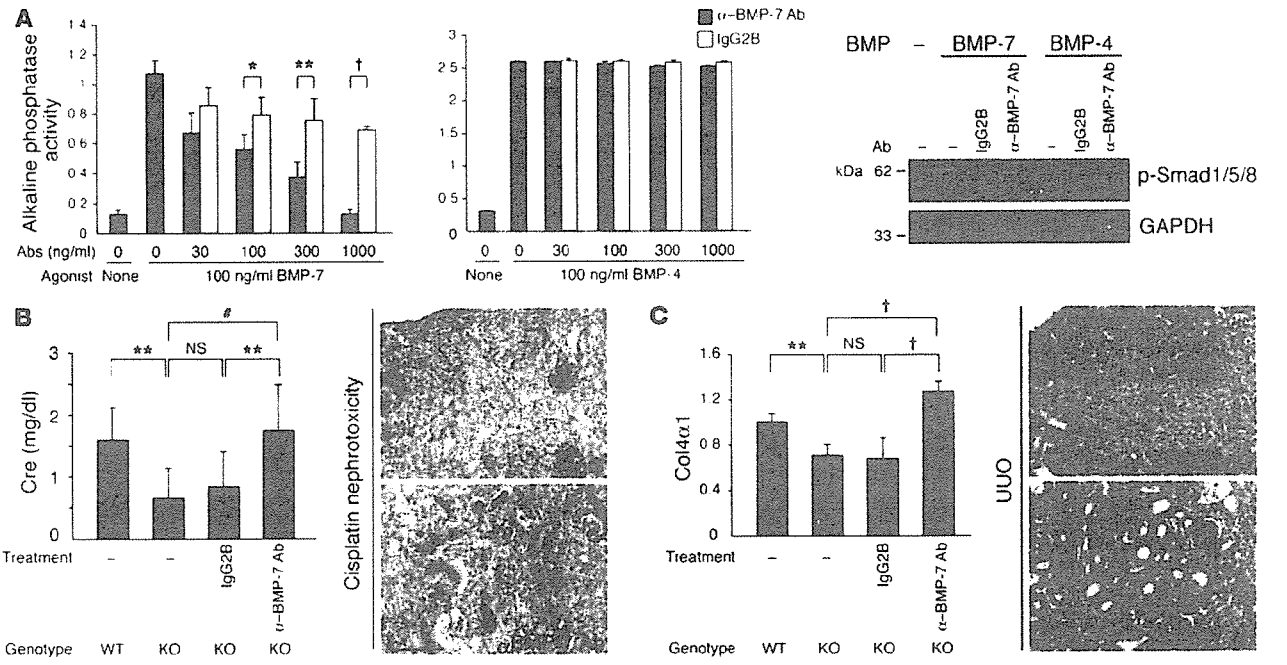

Figure 5

Blocking BMP-7 activity abolishes renoprotection in *USAG1*$^{-/-}$ mice. (**A**) Evaluation of neutralizing activity of anti–BMP-7 antibody. Anti–BMP-7 antibody inhibits alkaline phosphatase activity and phosphorylation of Smad1/5/8 induced by BMP-7, but not by BMP-4. (**B**) Serum creatinine level of *USAG1*$^{-/-}$ mice treated with anti–BMP-7 antibody and representative histological findings on day 3 of cisplatin nephrotoxicity. Scale bar: 100 μm. (**C**) Gene expression of type IV collagen in kidneys of *USAG1*$^{-/-}$ mice treated with anti–BMP-7 antibody and representative histological findings on day 14 of UUO. $^{*}P < 0.1$; $^{**}P < 0.01$; $^{\#}P < 0.001$; $^{\dagger}P < 0.0001$.

Discussion

Epithelial-mesenchymal transition (EMT) is a necessary step for renal fibrosis, as well as in embryonic development and tumor progression (29–31). TGF-β is known to stimulate EMT, while BMP-7 inhibits and reverses the transition (3). Zeisberg et al. recently reported that BMP-7 reverses TGF-β1–induced EMT and induces mesenchymal-epithelial transition in vitro (4, 32). They further demonstrated that administration of a pharmacological dose of BMP-7 resulted in regression of established lesions in the kidney and improved renal function. In this report, we demonstrated that deficiency of USAG-1, a novel BMP antagonist in the kidney, results in marked preservation of renal function by reinforcement of BMP signaling.

Based on these findings, we set the working hypothesis: in many types of renal disease, proximal tubule epithelial cells (PTECs) are the main site of injury (33) and undergo EMT, which causes loss of structural integrity of epithelial cells characterized by a reduction of E-cadherin expression and the induction of α-SMA in interstitial myofibroblasts (Figure 7A). BMP-7 secreted from distal tubules (12) inhibits EMT of PTECs and induces redifferentiation of mesenchymal cells to epithelial cells. USAG-1 produced from distal tubules binds to BMP-7 and inhibits its renoprotective action by interfering with binding to its receptors.

In addition to the inhibition of EMT, many other pharmacological actions of BMP-7 have been reported. Administration of recombinant BMP-7 inhibits the induction of inflammatory cytokine expression in the kidney (12), attenuates inflammatory cell infiltration (6), and reduces apoptosis of tubular epithelial cells in renal disease models (34) (Figure 7A). These phenomena are also observed in *USAG1*$^{-/-}$ mice, and the similarity between BMP-7–treated animals and *USAG1*$^{-/-}$ mice strongly supports our working model that deficiency of USAG-1 reinforces the renoprotective activities of BMP.

In accordance with this hypothesis, the renoprotection in *USAG1*$^{-/-}$ mice was abolished in both renal disease models when a neutralizing antibody against BMP-7 was administered (Figure 5). These results strongly support the hypothesis, and BMP-7 is a potent candidate for the counterpart of USAG-1.

We also observed preserved phosphorylation of Smad1/5/8 in the kidneys of *USAG1*$^{-/-}$ mice in both renal disease models, suggesting that BMP signaling was enhanced in *USAG1*$^{-/-}$ mice, while no difference was observed between WT and KO mice in phosphorylation of Smad1/5/8 prior to disease induction (Figure 4, A and C). We assume that BMP signaling prior to disease induction might be potent enough to cause full phosphorylation of Smad1/5/8 regardless of the presence or absence of USAG-1, while in the later stages of kidney diseases, BMP signaling is decreased and the presence of USAG-1 might cause a further reduction in BMP signaling.

Furthermore, we demonstrated that USAG-1 is by far the most abundant BMP antagonist in the kidney (Figure 6A). Because other BMP antagonists also antagonize BMP-7 activities (Supplemental Figure 2), we conclude that USAG-1 plays an important role in the modulation of BMP activities in the kidney not because of its ligand specificity, but because of its high expression among other BMP antagonists. In addition, the tissue localization of USAG-1 (Figure 6B) is quite similar to that of BMP-7 (12), and USAG-1 can effectively access and inactivate BMP-7 at the site of production.

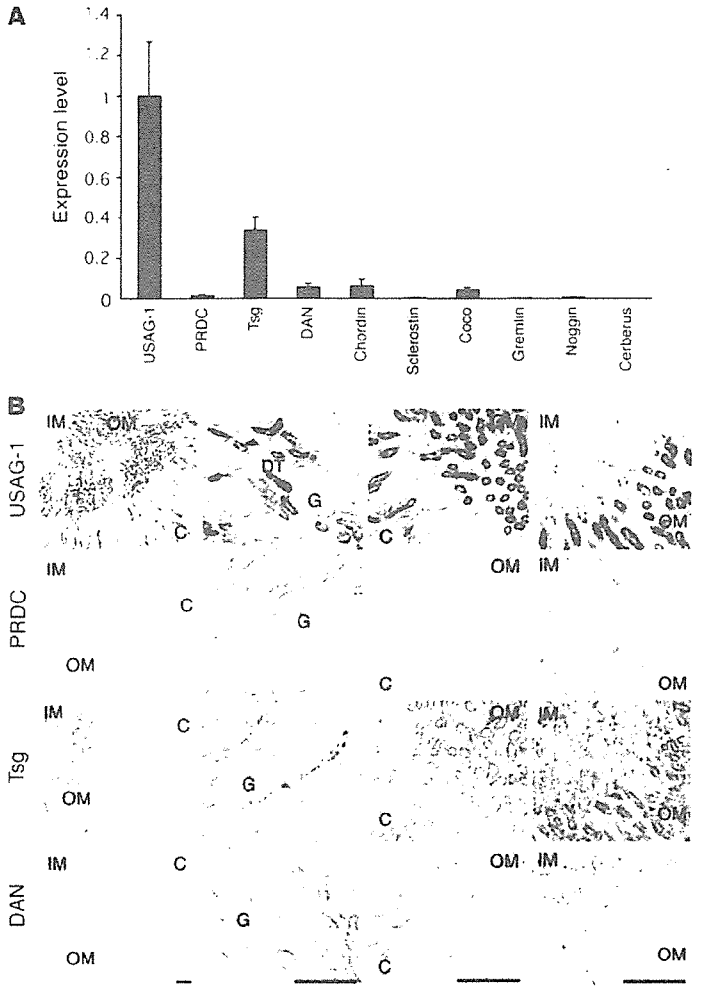

Figure 6
Expression of BMP antagonists in kidney. (**A**) Kidney cDNA of wild-type mice with Svj background was subjected to real-time PCR with various primers for BMP antagonists, and the standard curve was set using the plasmid encoding each BMP antagonist from concentrations of 1 pg/μl to 1 fg/μl. The values of each BMP antagonist in the kidney cDNA were multiplied by the length of the vectors and normalized to the value of USAG-1 expression (n = 4–5). Expression of USAG-1 was by far the most abundant in the kidney among other BMP antagonists. Tsg, twisted gastrulation. (**B**) Kidney sections were subjected to in situ hybridization with probes for all BMP antagonists. Expression of USAG-1 was confined to the distal tubular epithelial cells. Twisted gastrulation was also sparsely expressed in some distal tubules. Differential screening–selected gene aberrative in neuroblastoma (DAN) and protein related to DAN and Cerberus (PDRC) were faintly detected in the inner medulla. Expression of other BMP antagonists was not detected by this method. Scale bars: 100 μm. IM, inner medulla; OM, outer medulla; C, cortex; DT, distal tubule; G, glomerulus.

Although we illustrated USAG-1/BMP-7 binding as occurring outside of PTECs in Figure 7A, it might be possible that the binding occurs intracellularly within the secretory pathway in PTECs and that USAG-1 and BMP-7 are secreted in complex form. Further investigations are necessary to clarify this point.

Interestingly, the expression of USAG-1 decreased during the course of disease models (Supplemental Figure 3 and unpublished observations). We assume that the reduction of USAG-1 in renal diseases is a self-defense mechanism to minimize its inhibitory effect on BMP signaling. Because the reduction in USAG-1 expression in WT mice is not enough to overcome the reduction in BMP-7 expression, further reduction or abolishment of the action of USAG-1 is desirable for the preservation of renal function, and the results of the present study justify therapy targeted toward USAG-1. For example, drugs or neutralizing antibodies that inhibit binding between USAG-1 and BMP or gene-silencing therapy for *USAG1* would enhance the activity of endogenous BMP and might be a promising way to develop novel therapeutic methods for severe renal disease (Figure 7B). Because the expression of USAG-1 is confined to the kidney in adult mice and humans (21), it would be a better target for kidney-specific therapeutic trials. On the other hand, administration of recombinant BMP-7, whose target cells are widely distributed throughout the body, might produce some additional extrarenal actions, including beneficial effects, such as actions on renal osteodystrophy (35–39) and vascular calcification (40, 41).

Furthermore, these therapies targeted toward USAG-1 might protect the kidney during administration of nephrotoxic agents such as cisplatin. The pathological roles of USAG-1 in glomerular injury should be further elucidated before we undertake therapeutic trials against USAG-1.

Despite the essential role of BMP-7 in renal development, we did not observe any developmental abnormality in the kidney of *USAG1*$^{-/-}$ mice with this genetic background. We assume that there are many reasons for the lack of developmental abnormality: First, USAG-1 expression in the developing kidney is not apparent on embryonic day 11.5 (21), whereas BMP-7 expression is intense in the metanephric mesenchyme (42) with a pattern similar to that of gremlin (43). In the later stages, USAG-1 expression appears in the tubular epithelium in the medullary region (21), whereas BMP-7 expression is confined to the condensed mesenchyme and peripheral ureteric epithelium (42). Therefore, the expression pattern of USAG-1 in the developing kidney is totally different from that of BMP-7. Second, the expression of USAG-1 is very low in early embryogenesis, increases toward the late stage of embryogenesis, and is much higher in the adult kidney (21), while the expression of gremlin is high in early embryogenesis with a pattern similar to that of BMP-7, and becomes almost undetectable in the healthy adult kidney (Figure 6). Furthermore, *gremlin*-deficient mice show severe developmental abnormality in the kidney, which is quite similar to that of *BMP-7*-deficient mice. Therefore, we conclude that gremlin is a regulator of BMP-7 activity in the developing kidney, and lack of USAG-1 might be compensated by gremlin and does not cause any developmental abnormality in the kidney.

Recently another function of USAG-1 as a modulator of Wnt signaling has been reported in *Xenopus* embryogenesis (44). Although the role of the Wnt pathway in the progression of renal diseases remains to be elucidated, there is a possibility that modulation of the Wnt pathway might also play some roles in the preservation of renal function in *USAG1*$^{-/-}$ mice. Close relationships between the Wnt and BMP pathways have also been reported; for instance, dickkopf homolog 1 (DKK1), a Wnt antagonist, and noggin, a BMP antagonist, cooperate in head induction, while the expression of

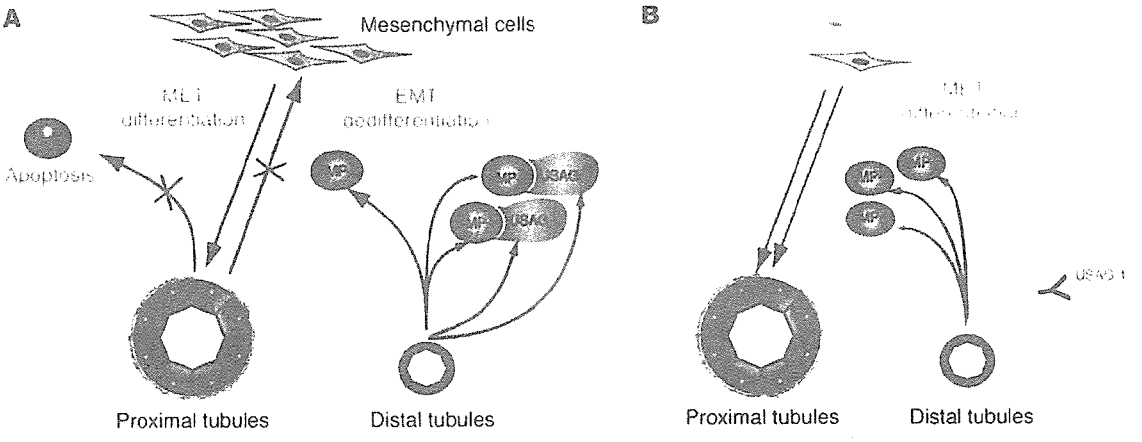

Figure 7
Working model of role of BMP-7 and USAG-1 in renal diseases. (**A**) In renal injury, PTECs are mainly damaged and undergo EMT to fibroblast-like mesenchymal cells. BMP-7 secreted by the distal tubule inhibits EMT and apoptosis of PTECs. USAG-1 is also secreted by the distal tubule, binds to BMP-7, and inhibits the renoprotective actions of BMP-7. (**B**) Therapeutic implication of USAG-1. Reduction of USAG-1 activity, for example, by a neutralizing antibody blocking the binding of USAG-1 and BMP-7, results in reinforcement of the renoprotective action of BMP-7. MET, mesenchymal-epithelial transition.

DKK1 is regulated by BMP-4 in limb development. Furthermore, a BMP antagonist, cerberus, has binding sites for both Wnt and BMP and antagonizes the activities of both the Wnt and BMP signaling pathways. USAG-1 might also have dual activities and act as a molecular link between these 2 important signaling pathways.

In conclusion, this study showed that USAG-1 plays important roles in the progression of renal diseases and might be a potent negative regulator of the renoprotective action of endogenous BMP signaling. Recently, Lin et al. identified a positive regulator of BMP-7 named kielin/chordin-like protein (KCP) and demonstrated that *KCP*$^{-/-}$ mice are susceptible to tubular injury and interstitial fibrosis (45). These data support the idea that BMP-7 protects the kidney from renal injury. Because these negative and positive modulators of BMP signaling regulate and edge the boundaries of BMP activity, further understanding of these modulators would give valuable information about their pathophysiological functions and provide a rationale for a therapeutic approach against these proteins.

Methods

Generation of USAG1$^{-/-}$ *mice.* We isolated a genomic fragment containing the mouse *USAG1* gene by screening a 129/SvJ genomic library (Stratagene). We inserted an *nlacZ* gene and a PGK-*Neo*R cassette in the opposite transcriptional orientation to the *USAG1* gene. ES cells were transfected with the linearized targeting vector by electroporation and selected by G418-containing medium. Homologous recombinants were screened and identified by genomic Southern blot analysis with an *Hin*cII-*Eco*RI probe mapping outside the 5′ homology arm (Figure 1A). Homologous recombined ES cell clones were obtained, and correct recombination was confirmed by Southern blot (Figure 1B) as well as PCR analyses. ES cells carrying the *USAG1*-null allele were injected into C57BL/6 blastocysts to obtain chimeric mice, which were crossed with wild-type C57BL/6J mice. Following germline transmission, the mice were maintained in a mixed SvJ background. PCR genotyping was used for all subsequent studies to allow specific detection of both the wild-type and *USAG1*$^{-/-}$ alleles (Figure 1C). Sequences of the primers used for genotyping are as follows: F1, CCCCTCCTCATCTGGCTGCTTCCTAAACGG; R1, CAGTCACGACGTTGTAAAACGACGGGATCC; F2, GGGATCCCACCCCTTCTCT; and R2, GCCGGGACAGGTTTAACCA.

Animal use. All experiments except those represented in Supplemental Figure 3 were performed using *USAG1*$^{-/-}$ mice and their wild-type littermates (*USAG1*$^{+/+}$) of the F_2 generation. All mice were housed in specific pathogen-

Table 1
Primers for real-time RT-PCR

Gene	Sequence of primers (5′-3′)
GAPDH	CCAGAACATCATCCCTGCATC; CCTGCTTCACCACCTTCTTGA
TNFα	ATGAGAAGTTCCCAAATGGCC; CCTCCACTTGGTGGTTTGCTA
IL-1β	CCTTCCAGGATGAGGACATGA; AACGTCACACACCAGCAGGTT
TGFβ1	GCAACAATTCCTGGCGTTACC; CGAAAGCCCTGTATTCCGTCT
MCP-1	TGCATCTGCCCTAAGGTCTTC; AAGTGCTTGAGGTGGTTGTGG
Col4α1	TTCCTTCGTGATGCACACCA; TTCTCATGCACACTTGGCAGC
USAG1	GCAACAGCACCCTGAATCAAG; TGTATTTGGTGGACCGCAGTT
Chordin	GCAGTGGTTCCCAGAGAATCA; AACAATCGTCCCGCTCACAGT
DAN	CTTCAGTTACAGCGTCCCCAA; CCAAGGTCACAATCTCCCACA
PRDC	AGGAGGCTTCCATCTCGTCAT; CCGGTTCTTCCGTGTTTCA
Twisted gastrulation	AAACGTGTCTGTTCCCAGCAA; ACACTGGTGGATGGACATGCA
Gremlin	AGCCCAAGAAGTTCACCACCA; TATGCAACGGCACTGCTTCAC
Sclerostin	CAAGCCTTCAGGAATGATGCC; TCGGACACATCTTTGGCGT
Noggin	AGAAACAGCGCCTGAGCAAGA; AAAAGCGGCTGCCTAGGTCAT
Cerberus	CCCATCAAAAGCCACGAAGT; CCAAAGCAAAGGTTGTTCTGG
Coco	TCCGCTTTTAGCCACTAGGTG; GCTGTTATTCTGGTGTCCCCA
BMP-2	TCGACCATGGTGGCCGGGACCCG; TGTTCCCGGAAGATCTGGAGT
BMP-3	AGCGAATGGATTATCTCTCCCA; TCTTTTCCGGCACACAGCA
BMP-4	CTGGAATGATTGGATTGTGGC; GCATGGTTGGTTGAGTTGAGG
BMP-5	AAGCCTGCAAGAAGCACGAA; GGAAAAGAACATTCCCCGTCA
BMP-6	CCAACCACGCCATTGTACAGA; GGAATCCAAGGCAGAACCATG
BMP-7	TGTGGCAGAAAACAGCAGCA; TCAGGTGCAATGATCCAGTCC

free conditions. Experiments represented in Supplemental Figure 3 were performed using C57BL/6 mice. All animal experiments were approved by the Animal Research Committee at the Graduate School of Medicine, Kyoto University, and the Animal Experiment and Use Committee at the University of Tsukuba and were in accordance with NIH guidelines.

Cisplatin administration. Cisplatin (Sigma-Aldrich) was administered at 20 mg/kg to mice by a single intraperitoneal injection. Mice were sacrificed 72 hours after administration of cisplatin, and tissue and blood were collected for further analysis.

UUO. Complete UUO was performed as previously described (46). Briefly, under sodium pentobarbital anesthesia, the middle portion of the left ureter was ligated and cut between 2 ligated points. At 14 days after surgery, the mice were sacrificed, and the obstructed kidneys were subjected to the studies described below.

Histological studies. The kidneys were fixed in Carnoy solution and embedded in paraffin. Sections (2 μm) were stained with PAS for routine histological examination, and the degree of morphological changes was determined using light microscopy. The following parameters were chosen as indicative of morphological damage to the kidney after cisplatin injection and UUO: brush border loss, tubule dilatation, tubule degeneration, and tubule necrosis. These parameters were evaluated on a scale of 0 to 4, and classed as: 0, not present; 1, mild; 2, moderate; 3, severe; and 4, very severe. The remaining kidney was used for immunohistochemical study, RNA isolation, and protein extraction.

Immunostaining. Frozen sections of kidneys were subjected to immunostaining with polyclonal antibodies against type IV collagen (ICN Pharmaceuticals), phosphorylated Smad1/5/8 (Cell Signaling Technology), and phosphorylated Smad2/3 (Santa Cruz Biotechnology Inc.) and monoclonal antibodies against α-SMA (Sigma-Aldrich) and Mac-1 (BD Biosciences – Pharmingen) as previously described (47, 48).

Immunoblotting. Whole kidney protein was homogenized in RIPA buffer (50 mM Tris at pH 7.5, 150 mM NaCl, 1% Nonidet P-40, 0.25% SDS, 1 mM Na_3VO_4, 2 mM EDTA, 1 mM PMSF, and 10 μg/ml aprotinin) and subjected to immunoblotting as described previously (49). Anti-E-cadherin antibody and anti-GAPDH antibody were from BD Biosciences – Transduction Laboratories and Research Diagnostic Inc., respectively.

Apoptosis detection and quantification. The TUNEL technique (In Situ Cell Death Detection Kit; Roche Diagnostics GmbH) was used to detect apoptotic cells in situ. All apoptotic nuclei within a transverse section at the renal pelvis were counted.

Quantification of mRNA by real-time RT-PCR. Real-time RT-PCR was performed with a 7700 Sequence Detection System (Applied Biosystems). Five micrograms of total RNA was reverse transcribed in a reaction volume of 20 μl using Superscript III reverse transcriptase and random primers (Invitrogen Corp.). The product was diluted to a volume of 400 μl, and 5-μl aliquots were used as templates for amplification using SYBR Green PCR amplification reagent (Applied Biosystems) and gene-specific primers. Specific primers for each gene transcript (listed in Table 1) were designed using Primer Express software version 2.0.0 (Applied Biosystems) and checked as to whether they showed a single peak in the dissociation curve. Serially diluted cDNA or plasmids encoding probes for in situ hybridization were used to generate the standard curve for each primer, and the PCR conditions were as follows: 50°C for 2 minutes, 95°C for 10 minutes, then 95°C for 15 seconds and 60°C for 1 minute for 40 cycles.

Administration of neutralizing antibody against BMP-7. In cisplatin nephrotoxicity, 1.5 mg/kg neutralizing anti-BMP-7 antibody (R&D Systems Inc.) was peritoneally injected into *USAG1*$^{-/-}$ mice 24 hours after injection of cisplatin. In UUO, 0.5 mg/kg neutralizing anti-BMP-7 antibody was injected every 3 days from day 2 to day 11. As a negative control, isotype-matched IgG2B (BD Biosciences) was injected at the same time points. Neutralizing activity of the antibody was evaluated by an assay measuring the production of alkaline phosphatase activity by C2C12 cells, as previously described (21).

In situ hybridization. The kidneys were excised from adult male mice and fixed in 4% paraformaldehyde in PBS. Frozen sections (5 μm thick) were treated with 1 μg/ml proteinase K in PBS at 37°C for 30 minutes and acetylated in 0.1 M triethanolamine-HCl, 0.25% acetic anhydride for 15 minutes. Hybridization was performed with probes at concentrations of about 1 μg/ml in a hybridization solution (50% formamide, ×5 SSC, 1% SDS, 50 μg/ml transfer RNA, and 50 μg/ml heparin) at 60°C for 16 hours. RNA probes were synthesized by in vitro transcription with a DIG RNA Labeling Mix (Roche Diagnostics Corp.). Each probe was designed to contain an open reading frame with the following length and G+C content: USAG-1, 1.0 kbp (G+C 52.6%); sclerostin, 1.5 kbp (61.7%); coco, 1.2 kbp (54.7%); DAN, 1.0 kbp (60.6%); twisted gastrulation, 0.7 kbp (55.1%); PRDC, 0.8 kbp (57.7%); chordin, 1.5 kbp (60.2%); gremlin, 0.9 kbp (50%); noggin, 0.7 kbp (64.7%); cerberus, 1.5 kbp (48.8%). Hybridization was detected using an anti-DIG AP conjugate (Roche Diagnostic Corp.) and NBT/BCIP solution (Roche Diagnostics Corp.).

Analysis of phenotype of adult teeth. Skeletal preparations of the maxillae and mandibles were made by soaking the mouse heads in 0.02% proteinase K in PBS at 37°C for 4 days after peeling off the skin, dissecting the maxillae and mandibles, and clearing them in 5% H_2O_2 at room temperature for 5 minutes. Finally they were rinsed in H_2O and left to dry.

Statistics. All assays were performed in triplicate. Data are presented as mean ± SD. Statistical significance was assessed by ANOVA, followed by Fisher's protected least significant difference post-hoc test. Survival curves were derived using the Kaplan-Meier method and compared using log-rank test.

Acknowledgments

We are grateful to Y. Nabeshima, T. Nakahata, and T. Nakamura for helpful discussion. We are grateful to M. Yoshimoto for hematological evaluation of the mice. We thank A. Godo, H. Uchiyama, and A. Hosoya for technical assistance. We thank W. Gray for reading the manuscript.

Received for publication April 25, 2005, and accepted in revised form October 11, 2005.

Address correspondence to: Motoko Yanagita, COE Formation for Genomic Analysis of Disease Model Animals with Multiple Genetic Alterations, Graduate School of Medicine, Kyoto University, Shogoin Kawahara-cho 54, Kyoto 606-8507, Japan. Phone: 81-75-751-3465; Fax: 81-75-751-3574; E-mail: motoy@kuhp.kyoto-u.ac.jp.

1. Eddy, A.A. 1996. Molecular insights into renal interstitial fibrosis. *J. Am. Soc. Nephrol.* **7**:2495–2508.
2. van Kooten, C., Daha, M.R., and van Es, L.A. 1999. Tubular epithelial cells: a critical cell type in the regulation of renal inflammatory processes. *Exp. Nephrol.* **7**:429–437.
3. Neilson, E.G. 2005. Setting a trap for tissue fibrosis. *Nat. Med.* **11**:373–374.
4. Zeisberg, M., et al. 2003. BMP-7 counteracts TGF-beta1-induced epithelial-to-mesenchymal transition and reverses chronic renal injury. *Nat. Med.* **9**:964–968.
5. Vukicevic, S., et al. 1998. Osteogenic protein-1 (bone morphogenetic protein-7) reduces severity of injury after ischemic acute renal failure in rat. *J. Clin. Invest.* **102**:202–214.
6. Hruska, K.A., et al. 2000. Osteogenic protein-1 prevents renal fibrogenesis associated with ureteral obstruction. *Am. J. Physiol. Renal. Physiol.* **279**:F130–F143.
7. Hruska, K.A. 2002. Treatment of chronic tubulointerstitial disease: a new concept. *Kidney Int.* **61**:1911–1922.
8. Zeisberg, M., et al. 2003. Bone morphogenic protein-7 inhibits progression of chronic renal fibrosis associated with two genetic mouse models. *Am. J. Physiol. Renal. Physiol.* **285**:F1060–F1067.

9. Dudley, A.T., Lyons, K.M., and Robertson, E.J. 1995. A requirement for bone morphogenetic protein-7 during development of the mammalian kidney and eye. *Genes Dev.* **9**:2795–2807.
10. Luo, G., et al. 1995. BMP-7 is an inducer of nephrogenesis, and is also required for eye development and skeletal patterning. *Genes Dev.* **9**:2808–2820.
11. Ozkaynak, E., et al. 1990. OP-1 cDNA encodes an osteogenic protein in the TGF-beta family. *EMBO J.* **9**:2085–2093.
12. Gould, S.E., Day, M., Jones, S.S., and Dorai, H. 2002. BMP-7 regulates chemokine, cytokine, and hemodynamic gene expression in proximal tubule cells. *Kidney Int.* **61**:51–60.
13. Simon, M., et al. 1999. Expression of bone morphogenetic protein-7 mRNA in normal and ischemic adult rat kidney. *Am. J. Physiol.* **276**:F382–F389.
14. Wang, S.N., Lapage, J., and Hirschberg, R. 2001. Loss of tubular bone morphogenetic protein-7 in diabetic nephropathy. *J. Am. Soc. Nephrol.* **12**:2392–2399.
15. Lund, R.J., Davies, M.R., and Hruska, K.A. 2002. Bone morphogenetic protein-7: an anti-fibrotic morphogenetic protein with therapeutic importance in renal disease. *Curr. Opin. Nephrol. Hypertens.* **11**:31–36.
16. Almanzar, M.M., et al. 1998. Osteogenic protein-1 mRNA expression is selectively modulated after acute ischemic renal injury. *J. Am. Soc. Nephrol.* **9**:1456–1463.
17. Massague, J., and Chen, Y.G. 2000. Controlling TGF-beta signaling. *Genes Dev.* **14**:627–644.
18. Simmons, D.G., and Kennedy, T.G. 2002. Uterine sensitization-associated gene-1: a novel gene induced within the rat endometrium at the time of uterine receptivity/sensitization for the decidual cell reaction. *Biol. Reprod.* **67**:1638–1645.
19. Avsian-Kretchmer, O., and Hsueh, A.J. 2004. Comparative genomic analysis of the eight-membered ring cystine knot-containing bone morphogenetic protein antagonists. *Mol. Endocrinol.* **18**:1–12.
20. Laurikkala, J., Kassai, Y., Pakkasjarvi, L., Thesleff, I., and Itoh, N. 2003. Identification of a secreted BMP antagonist, ectodin, integrating BMP, FGF, and SHH signals from the tooth enamel knot. *Dev. Biol.* **264**:91–105.
21. Yanagita, M., et al. 2004. USAG1: a bone morphogenetic protein antagonist abundantly expressed in the kidney. *Biochem. Biophys. Res. Commun.* **316**:490–500.
22. Schrier, R.W. 2002. Cancer therapy and renal injury. *J. Clin. Invest.* **110**:743–745. doi:10.1172/JCI200216568.
23. Megyesi, J., Safirstein, R.L., and Price, P.M. 1998. Induction of p21WAF1/CIP1/SDI1 in kidney tubule cells affects the course of cisplatin-induced acute renal failure. *J. Clin. Invest.* **101**:777–782.
24. Ramesh, G., and Reeves, W.B. 2002. TNF-α mediates chemokine and cytokine expression and renal injury in cisplatin nephrotoxicity. *J. Clin. Invest.* **110**:835–842. doi:10.1172/JCI200215606.
25. Yang, J., and Liu, Y. 2001. Dissection of key events in tubular epithelial to myofibroblast transition and its implications in renal interstitial fibrosis. *Am. J. Pathol.* **159**:1465–1475.
26. Klahr, S., and Morrissey, J. 2002. Obstructive nephropathy and renal fibrosis. *Am. J. Physiol. Renal. Physiol.* **283**:F861–F875.
27. Chevalier, R.L. 1999. Molecular and cellular pathophysiology of obstructive nephropathy. *Pediatr. Nephrol.* **13**:612–619.
28. Sato, M., Muragaki, Y., Saika, S., Roberts, A.B., and Ooshima, A. 2003. Targeted disruption of TGF-beta1/Smad3 signaling protects against renal tubulointerstitial fibrosis induced by unilateral ureteral obstruction. *J. Clin. Invest.* **112**:1486–1494. doi:10.1172/JCI200319270.
29. Kalluri, R., and Neilson, E.G. 2003. Epithelial-mesenchymal transition and its implications for fibrosis. *J. Clin. Invest.* **112**:1776–1784. doi:10.1172/JCI200320530.
30. Bottinger, E.P., and Bitzer, M. 2002. TGF-beta signaling in renal disease. *J. Am. Soc. Nephrol.* **13**:2600–2610.
31. Iwano, M., et al. 2002. Evidence that fibroblasts derive from epithelium during tissue fibrosis. *J. Clin. Invest.* **110**:341–350. doi:10.1172/JCI200215518.
32. Zeisberg, M., Shah, A.A., and Kalluri, R. 2005. Bone morphogenic protein-7 induces mesenchymal to epithelial transition in adult renal fibroblasts and facilitates regeneration of injured kidney. *J. Biol. Chem.* **280**:8094–8100.
33. Gerritsma, J.S., van Kooten, C., Gerritsen, A.F., van Es, L.A., and Daha, M.R. 1998. Transforming growth factor-beta 1 regulates chemokine and complement production by human proximal tubular epithelial cells. *Kidney Int.* **53**:609–616.
34. Li, T., Surendran, K., Zawaideh, M.A., Mathew, S., and Hruska, K.A. 2004. Bone morphogenetic protein 7: a novel treatment for chronic renal and bone disease. *Curr. Opin. Nephrol. Hypertens.* **13**:417–422.
35. Davies, M.R., Lund, R.J., Mathew, S., and Hruska, K.A. 2005. Low turnover osteodystrophy and vascular calcification are amenable to skeletal anabolism in an animal model of chronic kidney disease and the metabolic syndrome. *J. Am. Soc. Nephrol.* **16**:917–928.
36. Gonzalez, E.A., et al. 2002. Treatment of a murine model of high-turnover renal osteodystrophy by exogenous BMP-7. *Kidney Int.* **61**:1322–1331.
37. Hruska, K.A., et al. 2004. Kidney-bone, bone-kidney, and cell-cell communications in renal osteodystrophy. *Semin. Nephrol.* **24**:25–38.
38. Lund, R.J., Davies, M.R., Brown, A.J., and Hruska, K.A. 2004. Successful treatment of an adynamic bone disorder with bone morphogenetic protein-7 in a renal ablation model. *J. Am. Soc. Nephrol.* **15**:359–369.
39. Simic, P., and Vukicevic, S. 2005. Bone morphogenetic proteins in development and homeostasis of kidney. *Cytokine Growth Factor Rev.* **16**:299–308.
40. Davies, M.R., Lund, R.J., and Hruska, K.A. 2003. BMP-7 is an efficacious treatment of vascular calcification in a murine model of atherosclerosis and chronic renal failure. *J. Am. Soc. Nephrol.* **14**:1559–1567.
41. Hruska, K.A., Mathew, S., and Saab, G. 2005. Bone morphogenetic proteins in vascular calcification. *Circ. Res.* **97**:105–114.
42. Godin, R.E., Takaesu, N.T., Robertson, E.J., and Dudley, A.T. 1998. Regulation of BMP7 expression during kidney development. *Development.* **125**:3473–3482.
43. Michos, O., et al. 2004. Gremlin-mediated BMP antagonism induces the epithelial-mesenchymal feedback signaling controlling metanephric kidney and limb organogenesis. *Development.* **131**:3401–3410.
44. Itasaki, N., et al. 2003. Wise, a context-dependent activator and inhibitor of Wnt signalling. *Development.* **130**:4295–4305.
45. Lin, J., et al. 2005. Kielin/chordin-like protein, a novel enhancer of BMP signaling, attenuates renal fibrotic disease. *Nat. Med.* **11**:387–393.
46. Nishida, M., et al. 2002. Absence of angiotensin II type 1 receptor in bone marrow-derived cells is detrimental in the evolution of renal fibrosis. *J. Clin. Invest.* **110**:1859–1868. doi:10.1172/JCI200215045.
47. Yanagita, M., et al. 2001. Gas6 regulates mesangial cell proliferation through Axl in experimental glomerulonephritis. *Am. J. Pathol.* **158**:1423–1432.
48. Yanagita, M., et al. 2001. Gas6 induces mesangial cell proliferation via latent transcription factor STAT3. *J. Biol. Chem.* **276**:42364–42369.
49. Yanagita, M., et al. 2002. Essential role of Gas6 for glomerular injury in nephrotoxic nephritis. *J. Clin. Invest.* **110**:239–246. doi:10.1172/JCI200214861.

ELSEVIER

Atherosclerosis 191 (2007) 440–446

ATHEROSCLEROSIS

www.elsevier.com/locate/atherosclerosis

Risk of coronary events in Japanese patients with both hypercholesterolemia and type 2 diabetes mellitus on low-dose simvastatin therapy: Implication from Japan Lipid Intervention Trial (J-LIT)

Shinichi Oikawa[a,*], Toru Kita[b], Hiroshi Mabuchi[c], Masunori Matsuzaki[d], Yuji Matsuzawa[e], Noriaki Nakaya[f], Yasushi Saito[g], Jun Sasaki[h], Kazuaki Shimamoto[i], Hiroshige Itakura[j],

The J-LIT Study Group

[a] *Nippon Medical School, Tokyo, Japan*
[b] *Kyoto University Graduate School of Medicine, Kyoto, Japan*
[c] *Kanazawa University Graduate School of Medicine, Kanazawa, Japan*
[d] *Yamaguchi University Graduate School of Medicine, Yamaguchi, Japan*
[e] *Sumitomo Hospital, Osaka, Japan*
[f] *Nakaya Clinic, Tokyo, Japan*
[g] *Chiba University Graduate School of Medicine, Chiba, Japan*
[h] *International University of Health and Welfare Graduate School, Fukuoka, Japan*
[i] *Sapporo Medical University School of Medicine, Hokkaido, Japan*
[j] *Ibaraki Christian University, Ibaraki, Japan*

Received 27 June 2005; received in revised form 4 April 2006; accepted 13 April 2006
Available online 12 June 2006

Abstract

Hypercholesterolemic patients with type 2 diabetes mellitus are at increased risk of coronary heart disease (CHD); however, direct evidence is very limited in Japanese patients. The J-LIT is the first nationwide study conducted to assess the relationship between serum lipid levels and development of coronary events in Japanese hypercholesterolemic patients. We analyzed the coronary events in the J-LIT study subjects by having type 2 diabetes or not. Of the total 41,801 subjects without prior CHD who received open-label simvastatin, 5 mg/day, 6554 (male 40.2%, age 57.8 ± 7.8) subjects had type 2 diabetes, while 35,247 (male 30.0%, age 57.8 ± 7.9) did not.

In this analysis, relative coronary event risks based on a 0.26 mmol/l (10 mg/dl) increase in low density lipoprotein-cholesterol (LDL-C), were similar between hypercholesterolemic subjects with and without type 2 diabetes (17.3% versus 19.4%). Although all subjects were treated with simvastatin, the subjects with type 2 diabetes have significantly more coronary events compared to the subjects without type 2 diabetes (1.80/1000 and 0.76/1000 patient-years, respectively). Given the results above, to reduce the risk of coronary events in Japanese patients with both hypercholesterolemia and type 2 diabetes, careful and strict cholesterol management is needed in addition to the control of blood glucose.

Keywords: J-LIT; Hypercholesterolemia; Type 2 diabetes; Coronary disease; Myocardial infarction; Simvastatin; Cohort study

* Corresponding author. Tel.: +81 3 3822 2131x7207/5802 8153; fax: +81 3 5802 8153.
E-mail address: shinichi@nms.ac.jp (S. Oikawa).

0021-9150/$ – see front matter © 2006 Elsevier Ireland Ltd. All rights reserved.
doi:10.1016/j.atherosclerosis.2006.04.017

Hypercholesterolemia is a significant risk factor for coronary heart disease (CHD) [1–4], and the risk of CHD-related events is five to seven times higher in patients with atherosclerotic diseases than subjects without them. Therefore, reducing the total cholesterol (TC) level is critical for the patients with atherosclerotic diseases [5,6]. In the previous reports [7,8], we demonstrated the clear relationship between low density lipoprotein-cholesterol (LDL-C) levels and CHD risk in the Japanese subjects. Lifestyle factors, such as diet and exercise, have strong influences on the risk of CHD development. While the incidence of CHD in Japan is still much lower than that in western countries [9,10], TC levels in Japanese people have been increasing, probably due to the westernized lifestyles (e.g., increased intake of animal fats and proteins) [11,12], which might subsequently increase the incidence of CHD. The westernized lifestyle might also be one of the major reasons that type 2 diabetes mellitus, has also been increasing dramatically over the past 20–30 years in Japan [13]. Type 2 diabetes is also well-established as a risk factor for the development of CHD.

Many investigators in the western countries have reported that patients with both hypercholesterolemia and type 2 diabetes have more increased risk for the incidence of coronary events (acute myocardial infarction and sudden cardiac death) compared to patients with hypercholesterolemia alone (reviewed in Ref. [14]). However, there is no data on this issue in Japan based on a large scale epidemiological survey. Therefore, it is worthwhile to analyze the J-LIT (Japan Lipid Intervention Trial) study for this purpose. The J-LIT was the first nationwide observational cohort study in Japan with a large number of hypercholesterolemic patients treated in usual clinical practice, and it was designed to assess the relationship between the lipid levels and the incidence of CHD [15]. In Japan, cholesterol lowering therapy is well established; therefore placebo control group was not placed for ethical and practical reasons. J-LIT patients without prior CHD (myocardial infarction or angina pectoris) were classified into diabetic and non-diabetic groups and we analyzed the incidence of coronary events and coronary deaths. We also assessed the relationship between the incidence of coronary events and risk factors in the study period.

1. Research design and methods

The design of the J-LIT study was described previously [15]. The study involved 6500 general practitioners throughout the country and enrolled 52,421 patients including men aged 35–70 years and postmenopausal women under 70 years of age, with a TC level ≥5.69 mmol/l. Exclusion criteria were recent acute myocardial infarction (MI) or stroke within a month, uncontrolled diabetes mellitus, serious concomitant hepatic or renal disease, secondary hypercholesterolemia, malignancy or any illness with poor prognosis. Patients were selected throughout Japan and received open-label simvastatin, 5–10 mg/day. The dosing was decided according to the approved Japanese labeling of Lipovas®. Lipid levels, adverse events, and coronary events were monitored for 6 years. Another lipid-lowering agent was permitted to use when serum TC level did not show an adequate response to simvastatin monotherapy 10 mg/day.

The primary endpoints were coronary events, including acute MI and sudden cardiac death. All coronary events during the study period were assessed by the Endpoint Classification Committee. Each patient was informed of the study purpose, as well as drug efficacy and the need of long-term treatment. In this report, we used criteria for the diagnosis of type 2 diabetes established in 1999 by the Japan Diabetes Society (JDS), which are similar to the WHO type 2 diabetes diagnostic criteria.

1.1. Statistical analysis

All data were analyzed using survival analysis. For baseline patient characteristics, patients were classified into groups with and without type 2 diabetes. The average lipid levels were calculated using the data obtained throughout the study period. In the cases of the subjects who experienced any other diseases or coronary events after the enrollment of the study, the lipid data after the events were excluded from the calculation. For the risk of CHD events, patients were stratified according to average lipid levels (TC, LDL-C, TG, and HDL-C) during the treatment period. TC, LDL-C, TG and HDL-C were classified into discrete intervals of 0.52, 0.52, 0.56 and 0.26 mmol/l, respectively. Reference categories were set for the subgroups of the lowest lipid levels. Relative risks with 95% confidence intervals were calculated using the Cox proportional-hazard model [16] with adjustment for baseline characteristics (gender, age, hypertension, type 2 diabetes mellitus, fasting blood glucose, and smoking). For all statistical analysis, p values < 0.05 were considered significant. All statistical calculations were performed using SAS software (version 6.12, SAS Institute Inc., Cary, NC).

2. Result

2.1. Follow-up of subjects

Of the 52,421 patients enrolled in the J-LIT study, 47,294 patients were screened for the primary prevention cohort study [7]. In this investigation, data collected from 41,801 of the patients were used for analysis; 5493 patients were excluded for the following reasons: lack of follow-up data (932 patients), violation of inclusion criteria (63 patients), unwillingness to participate (6 patients), and incomplete data on covariates (4492 patients). In the 6 years from the date of enrollment, 31,370 patients were followed up by the investigators. The average length of follow-up was 5.39 years per subject.

Table 1
Baseline characteristics and lipid profiles of the subjects by diabetes status

	DM	Non-DM	p-Value
Number of patients	6554	35247	
Male gender (%)	40.2	30.0	<0.001
Age (years)	57.8 ± 7.8	57.8 ± 7.9	0.536
Obesity (%)[a]	39.5	32.5	<0.001
Hypertension (%)	46.1	45.9	0.691
ECG abnormality (%)	15.1	12.5	<0.001
Family history of CHD (%)	4.5	4.8	0.317
Smoking habit (%)	21.3	15.6	<0.001
Alcohol consumption (%)	33.9	28.0	<0.001
Exercise (%)	59.1	48.8	<0.001
Fasting blood glucose (mmol/l)	8.53 ± 3.12	5.31 ± 1.16	<0.001
Lipid profiles			
Baseline (mmol/l)			
TC	6.98 ± 0.90	6.97 ± 0.88	0.353
LDL-C	4.68 ± 0.85	4.72 ± 0.87	<0.001
HDL-C	1.32 ± 0.40	1.38 ± 0.39	<0.001
TG	2.56 ± 2.51	2.14 ± 1.76	<0.001

During treatment (mmol/l)		% Change		% Change	
TC	5.64 ± 0.81	−19.2	5.70 ± 0.75	−18.2	<.001
LDL-C	3.38 ± 0.76	−27.8	3.47 ± 0.75	−26.5	<.001
HDL-C	1.39 ± 0.35	+5.3	1.44 ± 0.35	+4.3	<.001
TG	2.04 ± 1.46	−20.3	1.81 ± 1.07	−15.4	<.001

DM, type 2 diabetes; ECG, electrocardiogram; CHD, coronary heart disease; TC, total cholesterol; LDL-C, low-density lipoprotein-cholesterol, TG, triglyceride; HDL-C, high-density lipoprotein-cholesterol. Data are mean ± S.D.
[a] Obesity, body mass index ≥ 25 kg/m^2.

2.2. Baseline characteristics of the study patients

Of the 41,801 patients included in this analysis, 6554 (15.7%) had type 2 diabetes. The baseline characteristics of the patients with and without type 2 diabetes mellitus are shown in Table 1. There are characteristic differences between the patients with and without type 2 diabetes. Proportions of male, and obesity, were higher in the patients with type 2 diabetes mellitus ($p < 0.001$). Also, the rate of performing casual exercise was higher in the patients with type 2 diabetes, probably because they had been encouraged taking exercise by physicians due to their high blood glucose.

In patients with type 2 diabetes mellitus, oral hypoglycemic agents were used in 40.5%, while insulin was used in 5.6% of them.

2.3. Lipid levels

Table 1 illustrates the lipid levels at baseline and during the treatment period in the diabetic and non-diabetic patients. As shown, the lipid levels were similar between the two groups except TG ($p < 0.001$). This suggests that simvastatin is effective for the treatment of hypercholesterolemia, in both patient groups.

2.4. Incidence of coronary events

A total of 207 coronary events occurred during the study period (Table 2). As predicted, the incidence rate of coronary events is markedly higher in the hypercholesterolemic patients with type 2 diabetes than in the subjects without

Table 2
Incidence of coronary events

	N (incidence rate)		Relative risk (95% CI)	p-Value
	DM	Non-DM		
Coronary events	62 (1.80)	145 (0.76)	2.38 (1.77–3.21)	<0.001
			2.11 (1.56–2.85)	<0.001[a]
Fatal	25 (0.73)	37 (0.19)	3.75 (2.26–6.22)	<0.001
			3.31 (1.98–5.51)	<0.001[a]
Non-fatal	37 (1.07)	108 (0.57)	1.91 (1.32–2.78)	<0.001
			1.70 (1.17–2.47)	0.006[a]

DM, type 2 diabetes; incidence rate/1000 patient-years; CI, confidence interval.
[a] Adjusted with age, sex.

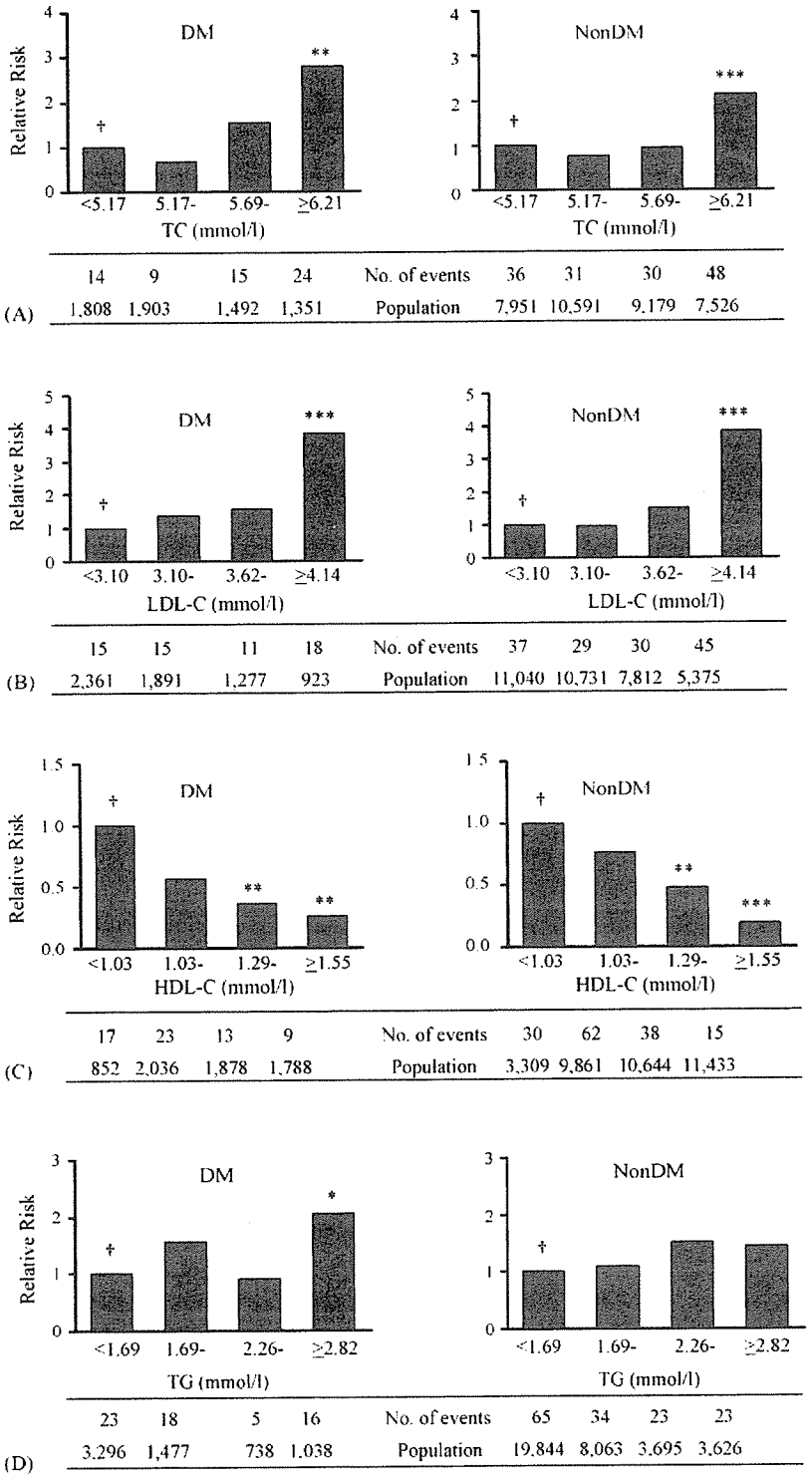

Fig. 1. Relative risk of coronary events based on lipid total cholesterol (TC) (A), low density lipoprotein-cholesterol (LDL-C) (B), high density lipoprotein-cholesterol (HDL-C) (C) and triglycerides (TG) (D) levels during treatment for patients with and without diabetes. Coronary events: myocardial infarction and sudden cardiac death. DM, type 2 diabetes. Adjusted with sex, age, hypertension, fasting blood glucose, and smoking habit.

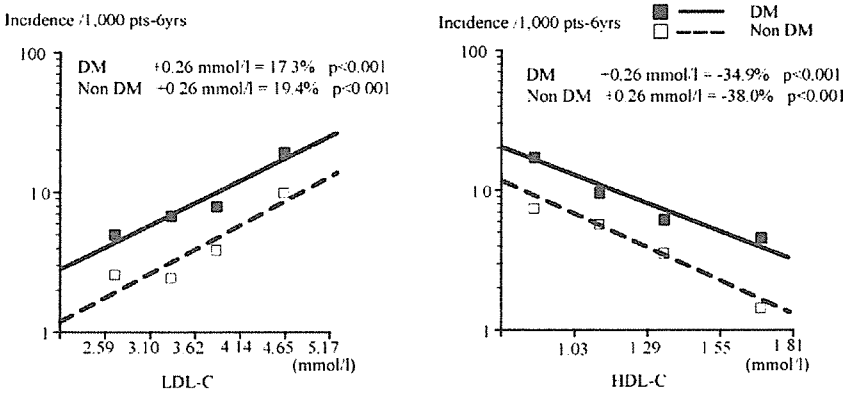

Fig. 2. The incidence of coronary events and lipid levels during treatment. Coronary events: myocardial infarction and sudden cardiac death. DM, type 2 diabetes. Adjusted with sex, age, hypertension, fasting blood glucose, and smoking habit.

it (1.8/1000 patient-years versus 0.76/1000 patient-years), despite ongoing treatment for type 2 diabetes during the study period. The relative risk of coronary event for type 2 diabetes was 2.38 (95% confidence interval 1.77–3.21, $p < 0.001$), and age and sex adjusted risk was 2.11 (95% CI 1.56–2.85, $p < 0.001$).

2.5. Relative risk of coronary events based on lipid levels during the treatment

Patients in both groups were stratified in four groups based on TC levels. Fig. 1(A) illustrates that the subgroups with TC levels higher than 6.21 mmol/l have significantly higher risk of coronary events in the both subjects with and without type 2 diabetes compared to those with TC < 5.17 mmol/l ($p = 0.003$ with type 2 diabetes and $p < 0.001$ without type 2 diabetes).

Patients in both groups were stratified in four groups based on LDL-C levels. Fig. 1(B) illustrates that the subgroups with LDL-C levels higher than 4.14 mmol/l have significantly higher risk of coronary events in the both groups with and without type 2 diabetes compared to those with LDL-C < 3.10 mmol/l ($p < 0.001$ in both groups).

Patients in both groups were stratified in four groups based on HDL-C levels. Fig. 1(C) illustrates that the subgroups with HDL-C levels higher than 1.29 mmol/l have significantly lower risk of coronary events in the both subjects with and without type 2 diabetes compared to those with HDL-C < 1.03 mmol/l ($p = 0.006$ and 0.003, respectively).

The relationship between the TG levels and coronary events risk is shown in Fig. 1(D). In patients without type 2 diabetes, the risk of coronary events does not differ based on TG level. On the other hand, in patients with type 2 diabetes, TG levels greater than 2.82 mmol/l showed two-fold increased risk of coronary events comparing to that of TG < 1.69 mmol/l ($p = 0.033$).

2.6. Relationship between lipid levels and the incidence of coronary events

The incidence of coronary event at different levels of LDL-C and HDL-C are illustrated in Fig. 2. For subjects with and without type 2 diabetes, an increase of 0.26 mmol/l (10 mg/dl) in LDL-C is associated with a 17.3 and 19.4% increase, respectively, in the risk of coronary events. On the other hand, an increase of 0.26 mmol/l (10 mg/dl) in HDL-C is associated with a 34.9% ($p < 0.001$) and 38.0% ($p < 0.001$) decrease, respectively, in the risk of coronary events. The association with an increase of 0.11 mmol/l (10 mg/dl) in TG and the risk of coronary events is weak (1.3%, $p = 0.051$ in type 2 diabetes and 1.2%, $p = 0.051$ in non-diabetes, respectively).

2.7. Relative risk of coronary events by baseline characteristics

The relative risks of coronary events analyzed by the patients' baseline characteristics are shown in Fig. 3. Male patients with hypercholesterolemia generally have more

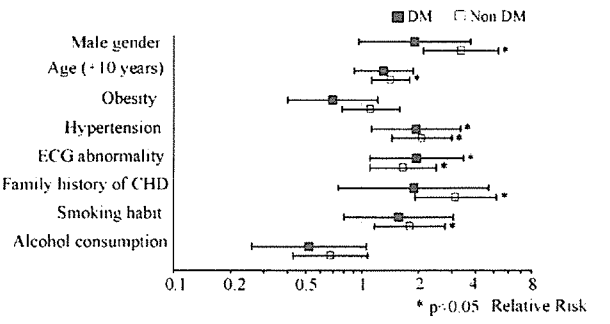

Fig. 3. Relative risk of coronary events by baseline characteristics. Coronary events: myocardial infarction and sudden cardiac death. Obesity, body mass index ≥ 25 kg/m^2; DM, type 2 diabetes. Adjusted with sex, age, hypertension, electrocardiogram abnormality, family history of CHD, smoking habit, and alcohol consumption.